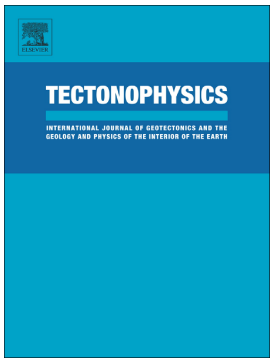

Forearc structure in the Lesser Antilles inferred from depth to the Curie temperature and thermo-mechanical simulations

Lydie Gailler, Diane Arcay, Philippe Münch, Guillaume Martelet, Isabelle Thinon, Jean-Frédéric Lebrun

PII: S0040-1951(17)30114-2
DOI: doi: 10.1016/j.tecto.2017.03.014
Reference: TECTO 127431

To appear in: *Tectonophysics*

Received date: 30 September 2016
Revised date: 10 March 2017
Accepted date: 21 March 2017

Please cite this article as: Lydie Gailler, Diane Arcay, Philippe Münch, Guillaume Martelet, Isabelle Thinon, Jean-Frédéric Lebrun , Forearc structure in the Lesser Antilles inferred from depth to the Curie temperature and thermo-mechanical simulations. The address for the corresponding author was captured as affiliation for all authors. Please check if appropriate. Tecto(2017), doi: 10.1016/j.tecto.2017.03.014

Forearc structure in the Lesser Antilles inferred from depth to the Curie temperature and thermo-mechanical simulations

Lydie *Gailler*[1, 2], Diane *Arcay*[3], Philippe *Münch*[3], Guillaume *Martelet*[4], Isabelle *Thinon*[4], Jean-Frédéric *Lebrun*[3]

[1] *Université Blaise Pascal, Laboratoire Magmas et Volcans, BP 10448, 63000 Clermont-Ferrand, France*

[2] *CNRS, UMR 6524, IRD, R 163, LMV, 6 Avenue Blaise Pascal TSA 60026 – CS 60026 63178 AUBIERE Cedex*

[3] *Université de Montpellier, CNRS, Université des Antilles, UMR 5243 Géosciences Montpellier, 34095 Montpellier Cedex 05, France*

[4] *Bureau de Recherche Géologique et Minière (BRGM), UMR 7327, 3 avenue Claude Guillemin, BP 36009, 45060 Orléans Cedex 2*

Abstract

Imaging deep active volcanic areas remains a challenge in our understanding of their activity and evolution, especially in subduction zones. Study of magnetic anomalies is appropriate to access such dynamics in depth. The magnetic anomaly pattern of the Lesser Antilles Arc (LAA) subduction is studied through Curie Point Depth (CPD), interpreted as the depth of the 580°C isotherm, and developed to better assess the deep thermal structure of the arc. The depth of the estimated CPD exhibits a complex topography. Keeping in mind the overall uncertainty associated with this method, a main doming is evidenced below the Guadeloupe archipelago. Its apex is shifted towards the ancient arc, suggesting a very hot state of the fore-arc/arc domain. To better understand the LAA thermal state, we perform 2D thermo-mechanical simulations of the subduction zone. Recalling that magnetite is a serpentinization by-product, we simulate water transfer triggered by slab dehydration to test the assumption of fore-arc serpentinization suggested by the positive magnetic anomaly in the vicinity of the Guadeloupe archipelago. In this area, the subduction-induced arc lithosphere hydration and

related weakening trigger a fast heating of the upper plate by basal convective removal. This process of fast arc lithosphere thinning may apply where simultaneously the volcanic arc is split in two and normal convergence is high enough. As serpentinization strongly decreases P-wave velocity, we propose a new interpretation of a published seismic profile below Guadeloupe. The seismic layer previously interpreted as the arc lower crust may rather be a layer of serpentinized mantle, as supported by spatial correlations between gravimetric and magnetic anomalies. Consequently, at the scale of Guadeloupe Island, the fore-arc Moho would be shallower than initially assumed, with a dome shape more consistent with both the extensive deformation active since the Oligocene in the inner fore-arc and the CPD doming.

Keywords

Lesser Antilles Arc; Magnetic anomaly spectral analysis; Curie Point Depth, Thermo-mechanical simulation, Water transfer, Serpentinization.

1. Introduction

Magnetic anomalies can provide information on lithology, temperature and hydration of the lithosphere, complementary to other geophysical techniques [*Manga et al.*, 2012; *Feuillet et al.*, 2010]. Sources of long wavelength magnetic anomalies were generally assumed to be concentrated in the crust, and mainly in the lower crust, implying that the lithospheric mantle contribution should be negligible [*Warner and Wasilewski*, 1995; *Wasilewski*, 1987; *Wasilewski and Mayhew*, 1992; *Wasilewski et al.*, 1979]. However, as proposed by *Dyment et al.* [1997], some recent works on mantle xenoliths *[Ferré et al*., 2013 and 2014] also suggest that the upper mantle may also contribute to magnetic anomalies. Spectral methods currently allow studying deep sources and have been used to provide additional information on mantle magnetization in various geodynamic settings: an old oceanic lithosphere [*Arnaiz-Rodríguez*

and Orihuela, 2013], a fore-arc region in a subduction zone [*Manea and Manea*, 2011], a hot spot area [*Gailler et al.*, 2016]. These studies are based on the determination of the Curie Point Depth (CPD) using classical spectral analysis of magnetic anomalies *[Spector and Grant*, 1970], with the assumption that crustal magnetization is a completely uncorrelated function of position [e.g., *Connard et al.*, 1983; *Blakely*, 1988; *Tanaka et al.*, 1999; *Ross et al.*, 2006]. More recent studies have introduced a more complex representation where crustal magnetization follows fractal behavior [e.g., *Pilkington et al.*, 1994; *Maus and Dimri*, 1995, 1996; *Maus et al.*, 2007; *Lovejoy et al.*, 2001; *Pecknold et al.*, 2001; *Gettings*, 2005; *Bouligand et al.*, 2009]. For both approaches, one may consider that these studies calculate a depth to the "magnetic sources bottom" rather than a "Curie Point Depth" sensu stricto [*Rajaram et al.*, 2009; *Ravat et al.*, 2011; *Salem* et al, 2014; *Wasilewski et al.*, 1979]. These two interfaces can differ for petrological reasons, lithological variations or because of structural effects. Nevertheless, such methods have been used to characterize regional thermal structures since Curie isotherm provides valuable information on both the present geothermal gradient, and the regional temperature field *[Arnaiz-Rodríguez and Orihuel*a, 2013; *Li et al*., 2013; *Bouligand et al*., 2009; *Blakel*y, 1988; *Campos-Enriquez et al*., 1990, 1989; *Shuey et al*., 1977]. To first order, the Curie point depth is a thermal boundary above which ferromagnetic minerals (the dominant carriers of magnetism) lose their ferromagnetic properties and become paramagnetic (e.g., the Curie temperature for magnetite is 580 °C). The lithosphere is therefore virtually nonmagnetic below the CPD. Numerous previous studies have found a CPD consistent with the geological contexts, being shallower in volcanic and geothermal areas, and deeper in stable continental areas [e.g. *Ates et al.*, 2005; *Bhattacharyya and Leu*, 1975b; *Blakely*, 1988; Connard *et al.*, 1983; *Okubo et al*., 1989, 1985; *Shuey et al.*, 1977; *Tsokas et al.*, 1998]. Several magnetic minerals may influence the magnetization of the upper mantle as summarized by *Ferré et al.* [2014]. However, their preliminary results suggest that magnetite is systematically present, and dominates the remnant magnetization of mantle xenoliths. With the depth of the Curie-temperature isotherm for ferromagnetic minerals lying well below the

crust-mantle interface in many geologic settings, a contribution of the mantle lithosphere to the magnetic signal is thus possible as also shown by *Gailler et al.* [2016].

In this work, we apply the determination of the CPD to the Lesser Antilles Arc (LAA), especially in its northern part, by combining data from global Earth Magnetic Anomaly Grid (EMAG2; [*Maus*, 2009]) and data from aeromagnetic surveys and marine campaigns recently compiled in the study area. This approach will help characterizing the regional thermal structures of the LAA but also better constraining the very complex structure of the fore-arc domain in its northern part where: (1) almost no heat flow data are available [synthesis in *Manga et al.*, 2012], (2) an oligocene–miocene remnant arc is present East of the present-day active volcanic arc, thus in a fore-arc setting [e.g., *Bouysse*, 1979; *Bouysse et al.*, 1985, 1988; *Bouysse and Westercamp, 1988*] and (3) extensional tectonics is active since at least the early Miocene [*Münch et al.*, 2014; *De Min et al.*, 2015]. One of the main goals of this study is therefore to better understand the origin of magnetic anomalies along the LAA subduction zone. In fore-arc settings it has been proposed that magnetic mantle may be common in relation with the serpentinization of the mantle wedge [*Blakely et al.*, 2005]. The serpentinization process, which is related to the hydration of the mantle wedge, generates the production of magnetite that contributes to long-wavelength magnetic anomalies above subduction zones [*Blakely et al.*, 2005]. In this paper we seek to improve the understanding of thermal and tectonic structures of the northern LAA taking into account that a remnant arc occurs in the present-day fore-arc domain.

To better interpret the inferred thermal structure, we perform complementary thermo-mechanical simulations to model the thermal structure of the fore-arc/arc domains in conditions close to steady state. The 2D numerical model includes a computation of water transfers, associated with slab dehydration/overlying rocks hydration and a simple water-induced mechanical weakening, in order to test (1) the hypothesis of fore-arc serpentinization

suggested by high magnetic anomalies and (2) its possible influence on the thermal state of the arc lithosphere. The time-scale given by the volcanic arc jump in the LAA (35 to 40 Ma ago) is used in this paper as a main constraint to discuss the modeling results, obtained for various mechanical parameters, convergence rates and initial hydration states. Our results are compared with the most recent geophysical interpretations and geodynamical models and lead us to propose a new interpretation of the structure of the volcanic arc domain in the northern part of the LAA.

2. Geodynamic setting and structure of the LAA

The LAA (Fig. l) is a 850-km long island arc which results from the oblique subduction of the North-and South-America plates beneath the Caribbean plate, at a mean rate of around 2 $cm.yr^{-1}$ in the SW direction relative to the Caribbean plate [*DeMets et al.*, 2001 and 2010]. The arc, convex towards the east, spans from 12°N to 18°N on the eastern edge of the Caribbean plate, and is made up of 20 islands carrying 21 active volcanoes with more than 34 historical eruptions [e.g. *Brid*e*n et al*., 1979; *Westercam*p, 1979]. To the East, an accretionary prism develops, especially in the southern part of the LAA, i.e., South of the island of Dominica, where it is known as the Barbados Ridge accretionary complex, and reaches there at most a 300 km width and a 20 km thickness. This thrust wedge results from the accretion of sediments since the Eocene and deformation under a compressional tectonic regime (Fig. l). Therefore, the LAA is generally considered as an accretionary convergent margin [*Clift and Vanucchi*, 2004; *Von Huene and Scholl*, 1991].

However, North of the island of Martinique, the arc displays a quite opposite tectonic regime: even if thrust earthquakes are common [*Gutscher et al.*, 2013], the accretionary prism is less developed, and the fore-arc domain is enlarged with eight main islands and numerous islets (Fig. 1). In this part of the subduction zone, the LAA separates into two sub-arcs (Fig. l) successively active since the late Oligocene. A westward displacement of the (active)

volcanic arc occurred in the late Oligocene, from an outer ancient arc ("Limestones Caribbean islands") to an inner arc ("Volcanic Caribbean islands"), active since ~20 Ma [*Bouysse and Westercamp, 1988*; *Bouysse et al.*, 1990]. This arc jump may be related to a slab breakoff at around 30 Ma [*Bouysse and Westercamp, 1988*; *Westbrook and McCann*, 1986]. The northern LAA exhibits an original configuration with an ancient arc located in the fore-arc domain of the present-day active arc. Moreover, in the northern LAA, the subduction zone was swept by three main aseismic ridges corresponding to oceanic fracture zones with a N130°E orientation, named, from North to South, the Barracuda Ridge, the Tiburon Ridge and the Ste Lucia Ridge (Fig. l). The two northern ridges have a topographic expression whereas the southernmost one is buried under the sediment cover and is only detected in seismic reflection profiles. The subduction of these ridges may be responsible for local uplifts in the fore-arc domain [*Bouysse and Westercamp, 1988*; *Feuillet et al.*, 2004]. Furthermore, *Bangs et al.* [2003] proposed that the subduction of the Tiburon ridge might have led to the deformation of the toe of the backstop resulting in (1) a weakly developed backthrust of the accretionary prism unlike as observed in accretionary convergent margins and in (2) the subduction of sediments beneath the backstop. The northern Lesser Antilles fore-arc domain is also characterized by recent to active arc-parallel extension that may result from slip partitioning and a strong coupling along the subduction interface [*Feuillet et al.*, 2002]. This area could be a distinct block with a slightly different motion compared to both Caribbean and North-America plates [*Lopez et al.*, 2006]. However, this proposal is still a matter of debate. *Symithe et al.* [2015] proposed on the contrary that no northern LAA block exists, because in this area the mechanical coupling (from a seismological point of view) along the subduction interface is assumed to be weak (uncoupled interface). In the north-central parts of the LAA, *Kopp et al.* [2011] imaged a laterally homogeneous crustal structure from the fore-arc up to the back-arc domain, with a flat and deep Moho, whose geometry does not appear consistent with the

shallow extensional tectonics. To sum up, the understanding of the northern LAA structure still needs to be improved, but appears to differ significantly from the one of southern LAA exhibiting typical features of an accretionary convergent margin.

Few studies using the magnetic anomalies aimed at improving the large-scale knowledge of the LAA structure [*Arnaiz-Rodriguez et al.*, 2013; *Gailler et al.*, 2013]. Using spectral analysis of the magnetic anomalies at the scale of the eastern Caribbean plate, *Arnaiz-Rodriguez et al.* [2013] have estimated the CPD from the maximum slope in the power spectrum. They showed that the CPD is relatively constant, with a large unperturbed area where the average CPD is 23 km, and proposed that the magnetic sources bottom was located in the upper mantle beneath the over-thickened oceanic crust of the Caribbean plate. In this study, *Arnaiz-Rodriguez et al.* [2013] also evidenced two shallow CPD areas: in the Venezuela basin (17 km) and in the northern LAA (18.5 km). They proposed that the CPD doming beneath the northern LAA was related to the high volcanic activity of this region. However the low resolution of the CPD mapping of *Arnaiz-Rodriguez et al.* [2013] does not allow detailing the structure of the overriding lithosphere in the northern LAA. In this paper, we combine magnetic data at both high and low resolutions to investigate the upper plate structure of the central and northern LAA.

2.1. Data

In this study, several magnetic datasets are compiled to build the presented large-scale total field magnetic anomaly map (Fig. 2). We used the complete dataset of *Gailler et al.* [2013] including the 1975 aeromagnetic survey of the overall archipelago [*LeBorgne and LeMouel*, 1976] initially merged at an altitude 1800 m, the offshore high-resolution magnetic data obtained during the Aguadomar survey (1998) and additional marine datasets (Arcante, 1980; Geoberyx, 2003; Kashallow cruises, 2009 and 2011), computed with a cell size of 800 m. More details are given in *Gailler et al.* [2013]. The data from global Earth Magnetic Anomaly

Grid (EMAG2, ~3 km in resolution) were used to significantly enlarge the study area in the oceanic domain [*Maus*, 2009]. The whole dataset has been corrected from the International Geomagnetic Reference Field (IGRF). All data were finally reduced at the EMAG2 4 km elevation with a good consistency between the different datasets. From a qualitative point of view, the magnetic scheme appears more complex in the northern part of the study area. At the scale of the emerged arc, Guadeloupe Island seems to mark a transition within the main magnetic signal. A negative east to west trend crosses the arc southern of Guadeloupe, limiting two main positive domains. The northern part is associated with a more complex signal suggesting interplay between complex sources and tectonic features as evidenced in *Gailler et al.* [2013]. At a larger scale, apart from the emerged volcanic zones, the study area is dominated by longer wavelength anomalies and their smoothness argues for a deep origin [*Gailler et al.*, 2013].

2.2. Methodology

The Curie Point Depth determination classically uses spectrum analysis techniques to separate the influences of various structures in the observed magnetic anomaly field. We use the approach of *Tanaka et al.* [1999] originally developed by *Okubo et al.* [1985], and based on the spectral technique of *Spector and Grant* [1970]. In this approach, using the high-wavenumber as well as low-wavenumber parts of the radially averaged power spectra allows for estimating the basal depth of the deepest sources. In a nutshell, the top bound and the centroid depths of a magnetic source, z_t and z_0, respectively, are calculated from the power spectrum of magnetic anomalies, and are used to estimate the basal depth of a magnetic source, z_b. z_t and z_0 are determined by fitting a linear regression through the high-wavenumber ($0.05 \times 2\pi < k < 0.2 \times 2\pi$ km^{-1}) and low-wavenumber ($k < 0.1 \times 2\pi$ km^{-1}) parts of the radially averaged spectrum of $ln\ (\phi_{\Delta T}\ (|k|)^{1/2})/(2\pi)$ and $ln\ (\phi_{\Delta T}\ (|k|)^{1/2}/|k|)/(2\pi)$, respectively (Fig. 3), ($|k|$ is the wavenumber and $\phi_{\Delta T}\ (|k|)$ is the spectrum of the magnetic anomaly). The basal depth, z_b,

was computed from equation 1, and was reduced to the sea level surface by subtracting 4 km to correct for the elevation of the magnetic anomaly map (Fig. 2).

$$z_b = 2z_0 - z_t \quad (1)$$

The radially averaged power spectra (Fig. 3) were calculated using the Magmap extension of Oasis Montaj software (Geosoft). The map was divided into square windows to study the lateral variations of the CPD. The dimensions of these windows should be based on a minimum ratio of 12:1 of the magnetic anomaly wavelength observed in surface, (related to the magnetic sources) [*Okubo et al.*, 1985]. Taking into account the wavelength of the main magnetic anomalies of our map, a window size of 120 x 120 km^2 was chosen. This is a trade-off between windows large enough to encompass large anomalies and small enough to achieve a detailed CPD map. The magnetic grid has been oversampled (cell size of about 470 m) for optimizing the Fourier transform approach. The windows overlap by 50 per cent in both the EW and NS direction. Accordingly, 226 windows were processed to derive the CPD values over the study area. An example of a power spectrum for an isolated window is given in Figure 3~~b~~. CPD estimates are computed for all magnetic areas over the entire map using the same wavelength for every window (Fig. 4a). The influence of window and cell size on CPD estimates are addressed in *Gailler et al.* [2016], showing that the calculated Curie surface fluctuates a little but an overall trend remains undoubtedly preserved providing an overall uncertainty of about 5 km on our CPD calculation.

However, we have to keep in mind the assumptions of the spectral potential field method presented in *Spector and Grant* [1970], and all its subsequent variants [Okubo et al. 1985; Fedi et al. 1997; Tanaka et al. 1999; Ravat et al. 2007; and Bansal et al. 2011] that use slope segments or peaks of spectra to derive depths of layers. The Tanaka method inherently assumes that magnetization is completely random (white spectrum). This assumption makes the theory simple, but if the behavior of the magnetization is significantly fractal in our study

area, then the true spectrum will decay more rapidly with increasing wavenumber than assumed by the Tanaka method, which will then yield a depth that is too deep [*Fedi et al.*, 1997; *Quarta et al.*, 2000; *Ravat et al.*, 2007; *Fedi*, 2016]. As mentioned in introduction, different publications have shown that fractal magnetization (red spectrum) can provide a better model for real magnetization distributions.

However, such approaches turned out difficult to apply in oceanic contexts. A comparison between both methods, *i.e.* centroid versus fractal estimation of the CPD, is presented in Supplementary data A. For the main range of wavelengths used to derive CPD values (*i.e.* $0<|k|<0.3$; Fig. 3), the shape of the real data spectrum lies close to the theoretical curve predicted by *Maus et al.* [1997] for a fractal magnetization of $\beta = 1$. Since such a value is in practice comparable to a non–fractal behavior of the magnetization [*Bouligand et al.*, 2009], we conclude that the assumptions of the centroid method, as used in this study, are valid for the study area. Also, as noise in the spectra can affect the quality of the CPD computation, we provide a map of misfit between the observed and the theoretical spectra for each CPD computation window. The theoretical radial power spectrum of magnetic anomalies derived from the shape of the Fourier radial power spectrum, as presented in this study, is derived from the following equation [e.g., *Connard et al.*, 1983; *Okubo et al.*, 1985; *Blakely*, 1988; *Tanaka et al.*, 1999; *Ross et al.*, 2006]:

$$\phi_{\Delta T}(k_H) = C'' - 2\,k_H\,zt + 2\,ln\,[1 - exp(-k_H\,\Delta z)] \qquad (2)$$

Where C'' is a constant and Δz *the* thickness of the horizontal slab within which magnetic sources are assumed to reside.

The misfit R between the theoretical curve expressed in (2) and the calculated radial power spectrum is defined as:

$$R = sqrt\,(1/N\ \Sigma\,(\phi_{\Delta T}\,calc\,(k_H) - \phi_{\Delta T}\,th\,(k_H))^2) \qquad (3)$$

Where N is the number of points in the calculated radial power spectrum.

For the LAA area, the calculated map of misfit is presented in figure 4b, displaying to the first order very low values indicating the good quality of spectra and therefore strengthening the CPD determinations. Also note that there is no correlation between the CPD variations and the misfit distribution: this observation is in favor of the good quality of our CPD map.

Another effect which can impact our CPD estimation is that the magnetic data used in this study come from an integration of several data sets, gathered at different resolutions (aeromagnetic, marine surveys and EMAG global model). Despite the care that was given to the preprocessing of our datasets, spectral analysis of data measured at different resolutions may influence CPD estimations. The influence of our combined dataset is discussed in Supplementary data B, showing that the calculated CPD is slightly underestimated in areas of high resolution datasets. However, we clearly show that the overall trend is similar between high and low resolution data with a mean difference of 3 km. As a consequence, relative variations of the CPD surface remain reliable and can be confidently interpreted. Integrating high resolution datasets remains also useful to preserve the accuracy of magnetic information in more complex areas such as volcanic islands.

2.3. Results

The interpolated CPD values vary between ~18 and 32 km, with a mean value of ~26 km (Figure 4a). This mean value is consistent with the one of 23 km proposed by *Arnaiz-Rodriguez and Orihuela* [2013] at a larger scale for the eastern Caribbean. At the scale of the study area, an overall good consistency is evidenced between our CPD results and those from *Arnaiz-Rodriguez and Orihuela* [2013]. The main discrepancies are observed in areas distant from the arc and could be attributed to the different methods used by *Arnaiz-Rodriguez and Orihuela* [2013] as well as to the larger windows which may therefore overlap several sources. Considering a mean crustal thickness of 15–20 km for the Caribbean plate [*Edgar et*

al., 1971; *Houtz and Ludwig*, 1977; *Ladd and Watkins*, 1980; *Officer et al.*, 1959], the CPD would thus be mainly located within the upper mantle beneath the Caribbean plate, implying that the upper part of the mantle should be magnetized. In the back-arc domain, the CPD is deep (~28 km depth on average), *i.e.*, located within the lithospheric mantle, except beneath the Aves Ridge where a secondary CPD minima (23 km depth) seems to occur north of the Aves Island. An interesting point is that the crust beneath the Aves Ridge, which corresponds to a paleo-arc [*Fox et al.*, 1971], is thickened probably up to 30 km [*Keary*, 1974, Fig. 4c]. However regarding the uncertainties reliable to the noise in the power spectra and since this area is defined by a limited number of CPD determinations, we do not provide interpretation for the secondary minima. Beneath the active arc, the CPD falls between 19 and 26 km and would be mainly located within the arc crust, if one considers a crustal thickness of 20-28 km [*Christeson et al.*, 2008; *Kopp et al.*, 2011]. The most striking anomalies correspond to two CPD minima (< 20 km depth) located in the central LAA, beneath the active arc (Guadeloupe and Martinique islands). The shallow anomaly beneath the Guadeloupe Island extends southeastwards in the fore-arc domain, consistently with the large-scale CPD map of *Arnaiz-Rodriguez and Orihuela* [2013]. In the fore-arc domain, where the shallowest doming (~18.5 km) of our CPD map occurs, the magnetic sources should be located in the crust assuming a thickness of the fore-arc crust in the vicinity of the Guadeloupe archipelago of 24-28 km [*Kopp et al.*, 2011]. Elsewhere in the fore-arc domain, three secondary CPD minimas are also observed: two near the northern termination of the arc and a third one beneath the Tobago fore-arc basin. Here again, these second order domings are constrained only by a limited number of CPD windows, and must thus be cautiously interpreted. Beneath the accretionary prism the CPD deepens down to ~32.5 km South of St Lucie aseismic ridge. Finally, the deep CPD (>26 km) beneath the oceanic subducting plate indicates that the incoming lithospheric mantle is magnetic, as the one beneath the oceanic Caribbean plateau.

Moreover, we have to keep in mind that CPDs can represent a lithological (instead of a thermal) boundary at a temperature lower than 580°. At the scale of the Lesser Antilles arc, the Moho depth is estimated between 24 and 34 km [*Sevilla et al.*, 2010; *Kopp et al.*, 2011]. We have therefore compared our CPD results with Moho depths, to verify that there is no straightforward correlation between the two datasets, as evidenced in Table 1. We have further performed this comparison using the Crust1.0 model (*Laske et al.*, 2013; http://igppweb.ucsd.edu/~gabi/rem.html). It displays no apparent correlation between Moho depth and CPD at the scale of the study area (Fig. 4c): the influence of crustal thickness variations on our CPD calculation is negligible at first order. We can thus conclude that the CPD variations are not compositional in first approximation but more likely reflect thermal effects, foreseeable in the highly active subduction context of the LAA.

To discuss more accurately CPD variations, four profiles are displayed (Fig. 5): two along the active and ancient arcs (profiles 1 and 2, respectively) and two perpendicular to the volcanic front in the central and northern LAA (profiles 3 and 4).

Profile 1 (Fig. 5), corresponding to the active arc, shows that the CPD is slightly shallower in northern Antilles (~22.5 km) than in Southern ones (~25 km). The most important Curie point upwelling corresponds to the doming beneath the Guadeloupe and Martinique Islands with a CPD close to 19 km. Another doming is modeled just east of the Anegada passage at the northern termination of the volcanic arc, while two moderate CPD shallowings occur beneath the Saint Vincent Island and Grenada-Kick'em Jenny volcanic zone (Fig. 5). Therefore, CPD shallowings occur mainly beneath volcanic active islands.

Profile 2 (Fig. 5) is located along the ancient arc which merges with the active arc South of Martinique Island. The northern LAA exhibits the shallowest rising (~18.5 km depth) of the CPD map characterized by a large wavelength, whose apex occurs in the fore-arc domain

South of Guadeloupe. Eventually, the CPD progressively rises along profile 2 northward up to the Guadeloupe archipelago fore-arc, then progressively deepens to the Anegada passage.

Profile 3 (Fig. 5) is perpendicular to the central LAA and passes between the Guadeloupe and Dominique islands where convergence is almost normal (subduction rate of 2 cm/yr). This profile, first, crosses the major CPD rising in the Lesser Antilles, and, second, is exactly located on the seismic velocity profile modeled by *Kopp et al.* [2011], depicted in Figure 5. The CPD is deep (27.5 km on average) in the back-arc domain, it rises rapidly beneath the active arc around 20 km depth and continues rising up to ~18.5 km depth almost beneath the ancient arc, then remains shallow (≤ 20 km) beneath the whole inner fore-arc, and eventually deepens from the outer fore-arc to the trench. Thus, in the Guadeloupe archipelago, the shallowest CPD is not evidenced right under the active volcanic arc but is shifted in the inner fore-arc domain, towards the ancient arc. In the arc and fore-arc domains, the CPD would be predicted to be located within the lower crust accordingly to the velocity model of *Kopp et al.* [2011]. Moreover, the inner fore-arc CPD doming appears consistent with the shallowing of the boundary between the middle and lower arc crusts imaged by *Kopp et al.* [2011, Fig. 5).

Profile 4 (Fig. 5), perpendicular to the trench, images the northern LAA where the subduction obliquity is high [56°; *Gripp and Gordon*, 2002] and the normal convergence rate is very low (1.1 cm/yr). Along this profile, the shallowest CPD (~21 km) is obtained in the vicinity of the oceanic trench and the Anegada passage which is a transcurrent plate boundary.

2.4. Comparison of CPD with heat flow measurements

As our CPD calculations are interpreted as either shallowings or deepenings of the 580°C isotherm within the upper lithosphere, we compare them to heat flow measurements (Fig. 4a). We used the dataset from *Manga et al.* [2012] representing a major improvement over the majority of previous measurements in this region [*Langseth and Grim*, 1964; *Nason and Lee*, 1964; *Vacquier and von Herzen*, 1964; *Langseth et al.*, 1966; *Epp et al., 1970*; *Clark et al.*,

1978] (Fig. 4). Most of these measurements are consistent, except the study of *Clark et al.* [1978] where measurements were based on probes that penetrated between 1.2 and 3.6 m and recorded only 2 or 3 temperature measurements, with no measure of ocean temperature. Accordingly, we do not consider these values and will focus on the measurements from *Manga et al.* [2012]. At first order correlation can be observed between our CPD results and the measurements from *Manga et al.* [2012]. According to *Manga et al.* [2012], a main high heat flow anomaly corresponds to the active arc and fore-arc domain (~0.08 W/m^2). We have to remember that high heat flow values are commonly attributed to volcanic and metamorphic regions (high thermal conductivities). Moreover, tectonically active regions generally affect the Curie point depth and heat flow values. This anomaly is well correlated with a doming of the CPD beneath the active arc. The deepening of the CPD in front of the subduction trench is consistent with the relatively low thermal gradient evidenced by *Manga et al.* [2012], commonly reported in similar contexts [*Schubert and Peter*, 1974]. Even at our scale, these evidences support CPD variations (or 580°C isotherm depth variations) as a witness of differences in thermal structure at the lithospheric scale. Accordingly, our CPD map reflects the shallowing or deepening of the 580°C isotherm within the upper lithosphere, and probably to some extent, the difference in crustal thickness, structure and petrology between the Lesser Antilles Arc and the regional oceanic environment. Therefore the CPD would rather be located in the upper mantle beneath oceanic crust (i.e. Caribbean plate, Grenada back-arc Basin and Atlantic lithospheres) and in the arc crust beneath the Aves Ridge and the LAA. This configuration is for example confirmed by *Li et al.* [2010] who have carried out a study in the South China Sea area where they found estimated depths to the magnetic bottom layer very correlative to surface heat flow. They conclude that dominant contributions to surface heat flow comes from incoming mantle heat flow due to thermal conduction. In continental

area, *Li et al.* [2012] also show that the mantle contribution slightly exceeds 70% of the total surface heat flow.

Despite the overall uncertainty associated to our CPD approach, we underline here significant information on the thermal state of the LAA, especially through the main doming at the scale of Guadeloupe Island. Accordingly, these results could be used as a first order trend for studying the thermal structure of the arc through thermo-mechanical models. In the following, we model the upper lithosphere thermal state by focusing on the fore-arc/arc/back-arc domain to address the thermo-mechanical conditions possibly leading to the CPD estimates computed here.

3. Thermo-mechanical simulations of the Lesser Antilles subduction zone

In this section, 2D numerical simulations modeling the structure of the Lesser Antilles subduction zone are performed in order to investigate, at first order, which set of thermo-mechanical conditions allows simulating the thermal state of the Lesser Antilles arc inferred from CPD calculations. Specifically, we aim at testing the parameters necessary to reproduce the thermal structure of the central and northern LAA, particularly of the Guadeloupe archipelago characterized by the major CPD doming in the inner fore-arc domain.

3.1. Model set-up

3.1.1. Initial state, boundary conditions, and thermo-mechanical code

We assume that the present-day geodynamic configuration of Lesser Antilles subduction zone (convergence rate, subduction dip angle, plate thickness) has remained more or less constant since 35 Ma, i.e. after the Oligocene volcanic arc jump. In the northern part of the Lesser Antilles, since the convergence obliquity progressively increases (from ~0° to 56°, [*Gripp and Gordon*, 2002]), the normal convergence rate reduces from 2 cm/yr (profile 4; 'Guadeloupe') to 1.1 cm/yr (profile 3; 'Saint Barth'). Simulations are performed along the CPD cross-sections 3 and 4 (locations on Figure 5). To mimic the Lesser Antilles subduction

zone structure, the subducting and overriding lithospheres are supposed to be ~100 km thick, this thickness corresponds to a 80 to >120 Ma old subducting lithosphere (Fig. 6a), as, for oceanic lithospheres older than ~70 Myr, basal small-scale convection stabilizes their thickness and thermal structure (e.g., Parsons and Sclater, 1977, Fleitout and Yuen, 1984, Dumoulin et al., 2001). We assume for the subduction plane an initial dip angle of 30° down to 55 km depth along both profiles [*e.g.*, Bijwaard, 1999].

Subduction experiments are performed using the finite element Eulerian code initially developed by *Christensen* [1984, 1992], solving equations of mass, energy, and momentum conservation for an incompressible fluid (extended Boussinesq approximation). Two different lithologies (crust/mantle) are tracked thanks to active tracers advected with the velocity field [*van Keken et al.*, 1997]. The 2D simulation box is 2220 km wide and 555 km high, filled with a mantle composition except on a 8.3 km thick layer overlying the future subducting lithosphere made of a weak and less dense material (gabbros, Fig. 6a), filling also the initial interplate channel. The computation of water transfers as a function of accurate phase transitions, yielding dehydration or hydration reactions, has been implemented [*Arcay et al.*, 2005]. Slip is free along the surface of the over-riding lithosphere while a constant subduction rate is imposed on the subducting plate, from the surface down to 13 km depth, far away from the subduction zone (Fig. 6a). The subducting lithosphere is continuously regenerated along the top left corner of the box following the method described in *Arcay et al.* [2008]. The bottom boundary is open to prevent the slab from rolling up when the diving plate reaches the box base. As convergence starts, strain localizes within the initial crustal and weak subduction plate, which (1) triggers the subducting plate bending and its subduction, (2) sustains a mechanical and kinematical decoupling between the two converging plates. Other thermal and mechanical boundary conditions are displayed in Figure 6a. The numerical resolution mesh is not regular, refined in the subduction zone where the cell x- and z-spacings are set to 1.66 km,

compared to 10.5 km elsewhere, and has been validated in a previous study (Arcay, 2017, in revision). The density of lithological tracers is uniform across the box (~2.63 per km^2) to respect a minimum (but sufficient, [*Arcay et al.*, 2005]) number of 7 markers in the smallest cell.

3.1.2. Hydration state of the upper lithosphere at simulation initiation.

Looking at the specificities of the Lesser Antilles subduction zone, we focus on the possible influence of the ancient arc located in the fore-arc domain, assumed to be responsible for extended serpentinization of the fore-arc mantle. Following *Bouysse and Westercamp* [1990], we assume that the volcanic arc jump results from a slab breakoff at around ~35 Ma and we simulate the present-day subduction state by applying a convergence rate constant since the Oligocene. We furthermore impose a pre-hydration of the fore-arc mantle in order to simulate the influence of the ancient arc (see below).

At subduction initiation, the incoming lithosphere is assumed to be water-satured down to 12 km depth: 2.97 wt% of water in the greenshist facies for the oceanic crust [*Bousquet et al.*, 1997] and 6.5 wt% in a 4 km-thick layer of serpentinised lherzolite imposed below the crust [*Schmidt et Poli*, 1998]. Water transfers are computed using (1) pressure-temperature (*P-T*) phase diagrams at water-saturation for either a gabbroic crust [*Bousquet et al.*, 1997] or a lherzolite composition [*Schmidt et Poli*, 1998], and (2) *P-T*-time path followed by each lithological marker. If a dehydration reaction is predicted to occur, the released water is assumed to percolate upwards instantaneously until reaching the nearest under-saturated marker. The remaining water achieving 11 km depth without having been absorbed is extracted from the simulation box, mimicking expelling by volcanism.

To test the impact of an assumed highly hydrated fore-arc domain, in relation to the westward arc jump, on the current arc thermal structure, the fore-arc mantle is initially water-saturated as follows. First, the geometry of the hydrated area in the fore-arc lithosphere is predicted by

using a water transfer simulation performed until steady-state (~540 km of convergence), with a subduction velocity of 1 and 2 cm/yr for the profiles 4 and 3, respectively. To simplify, these preliminary experiments were performed without water-related weakening (see section 4.1.3). In both cases, the resulting fore-arc hydration is discontinuous and made of two hydration patches as previously shown by *Arcay et al.* [2005]: the closer to the trench corresponding to hydration resulting from the subducting crust eclogitization, the further to the dehydration of the subducting mantle (Fig. 7a). As we cannot easily model the arc jump, we offset trenchward the water content distribution modeled in the preliminary experiments by 35 km in the case of profile 4 (Guadeloupe area; Fig. 6c) and 70 km in the case of profile 3 (St Barth area; Fig. 6d). Subduction is then initiated once again to simulate the present-day thermal state in the convergence zone. Subduction experiments are computed until reaching steady state conditions at the scale of the subduction zone. We focus on the times at which the 580°C isotherm shallows to either ~20 km depth, as indicated by CPD estimates, or 25 km to take into account the overall uncertainty in our CPD estimates (*i.e.* 5 km). For comparison, we also simulate the same subduction without a pre-hydration of the fore-arc mantle.

4.1.3. Rheological model

The modeled rheology combines a non-Newtonian behavior and a pseudo-brittle behavior. The simulated brittle strength (ν_b) depends on strain rate, $\dot{\varepsilon}$, and on a yield stress, τ_y, depending on composition, linearly increasing with depth (Fig. 6a and b). In the ductile realm, the viscous strength (viscosity labelled ν_v) depends on temperature (Arrhenius law), depth, composition (crust/mantle), strain rate (Fig. 6b, c), and water content (Fig. 6d). The effective rock viscosity, ν_{eff}, is computed assuming that the total strain rate is the sum of brittle and ductile deformations: $\nu_{eff}=(\nu_v^{-1}+ \nu_b^{-1})^{-1}$. We test two different parameter sets of ductile rheology for the anhydrous mantle. The first reference rheological parameter set (labeled Re) corresponds to that used by Arcay et al. [2008] to simulate the arc deformation regime

representative of most subduction zones. The second one corresponds to a stiffer mantle (rheology labeled St; [Arcay, 2012; Arcay, 2017, in revision] and is used to discuss the influence of the anhydrous viscosity law on the time scale of arc thermal thinning. To take into account the influence of water content ($[OH^-]$) on rheology, we apply a strength reduction depending exponentially on water content (Fig. 6d) that is identical for Re and St rheologies. This strength reduction reaches a maximum value (labelled f□when nominally hydrated phases such as amphibole, chlorite, and serpentine, are predicted to be stable (Arcay et al., 2005, Fig. 6d), i.e. when $[OH^-] \geq 0.5$ wt%. We test three different values of f_v (34.2, 50 and 100), already investigated for two of them (50 and 100) by Arcay et al. [2006].

3.2. Results

Figure 8 displays all performed experiments. In all simulations, the slab dehydration yields the water saturation of the overriding mantle wedge. Therefore, because we model a significant hydrous strength reduction, the base of the hydrated overriding lithosphere becomes gravitationally unstable and a small-scale convection (SSC) process initiates at ~28 Myr, sustained by the continuous slab dehydration [*Arcay et al.*, 2006]. This SSC brings about the conductive heating of the hydrated overriding lithosphere domain. As a result, the 580°C isotherm slowly shallows within the hydrated arc lithosphere.

3.2.1. Simulated thermal structure in the Guadeloupe island area: Effect of initial hydration state and rheology

Figure 7 highlights the thermal state evolution of the subduction zone performed with the reference mantle rheology and with (simulation G5, Fig. 7b) or without (simulation G4, Fig. 7a) a pre-hydration of the fore-arc mantle, whose water distribution is consistent with the kinematics observed across the Guadeloupe profile. As soon as the subducting slab dehydrates, the over-riding mantle is strongly hydrated by the formation of amphibole between ~1000°C and 700°C (figured by yellow to orange colors in Fig. 7a and 7b). In such early steps of experiments (14.9 Ma), serpentinization also develops but only in the pre-

hydrated case (figured by red color in Fig. 7b) at temperature below ~700°C. Without fore-arc pre-hydration, the simulated hydration window of the over-riding lithosphere is relatively narrow compared to faster convergence rates [*Arcay et al.*, 2005]. This probably limits SSC development and is likely to slow down the over-riding lithosphere thinning and heating processes. Consequently, the model predicts that the 580°C isotherm reaches 25 km and 20 km depth, ~165 km away from the trench, after 39.7 Ma and 44.3 Ma, respectively, of subduction (Fig. 7a). With a pre-hydration of the fore-arc mantle, the simulated hydration window is enlarged (Fig. 7b), becomes similar to the one simulated at high convergence rates [*Arcay et al.*, 2005]. The SSC initiation occurs earlier (22.3 Ma) and, therefore, the 580°C isotherm reaches 25 and 20 km depths more rapidly, i.e., after 28.7 Ma and 36.9 Ma respectively of convergence. Note that solely the basal and rather hot sublithospheric layer is involved in the convective destabilizing process. Nominally hydrated minerals such as serpentine are located at much shallower levels (T<700°C, i.e., at depth initially shallower than 37 km), meaning that the serpentinized and buoyant part of the upper lithosphere is not directly involved in the thermo-mechanical process.

Other simulations summarized in Figure 8 all show that the pre-hydration of the fore-arc mantle (solid symbols) accelerates the over-riding lithosphere thinning and heating. As expected, the amount of water-related weakening (f_ν) increases the rate of over-riding lithosphere thinning and heating (Fig. 8). It appears that $f_\nu \geq 50$ facilitate the simulation of a timing of lithosphere heating in agreement with the time-scale assumed for the Guadeloupe subduction segment (35 to 40 Ma BP). This maximum time-scale is verified in three experiments only (sim. G5, G8, and G9), all performed with the reference Rheology (Re), if the present-day depth of the 580°C is assumed to be 20 km. If the 580°C isotherm is assumed to be rather at 25 jm depth, then additional simulations G1, G4, and G11 verify the time constraint imposed by the LAA jump. Three simulations (G4, G8 and G11) corresponds to

experiments without fore-arc pre-hydration, among which for two of them f_v has to be set to a very high value (*i.e.* 100; Fig. 8), possibly too extreme [*Arcay*, 2012]. Indeed, this f_v value of 100 may apply to a strongly hydrated mantle (when serpentine is predicted to be stable) but might not correspond to an amphibole-bearing mantle (*i.e.*, modeled here for water content as low as 0.5%wt). However, as in our simulations the hydrous strength weakening is very simply modeled, the amount of water-related softening is constant (equal to f_v) from low to high water contents as soon as nominally hydrated phases are predicted. Only experiment G11 performed with rheology St shows an arc thinning and warming fast enough to simulate an 580°C isotherm upwelling in agreement with the present-day CPD uncertainty. Nevertheless, f_v in this case has to be set to the extreme value of 100. This result is not surprising, even if the rheology St appears to be a good proxy of experimental deformation measurements made on olivine (Fig. 6c): Recent studies on olivine rheology at low temperatures highlight the rather weak strength of olivine and argue for the use of a softer rheology [*Demouchy et al.*, 2013**,** *Boioli et al.*, 2015], such as rheology Re.

To sum up, taking into account an overall 5 km depth uncertainty on the CPD determination, six models could explain the general trend and the main observed CPD doming. The averaged doming at 20 km suggested by the CPD estimation could range between 15 and 25 km, but alternative depths are achieved by changing slightly the thermo-mechanical parameters. However, the most realistic conditions modeled to fit the subduction characteristics in the Guadeloupe segment correspond to simulations G1, G4 and G5 performed using a rather 'soft' anhydrous rheology (Re), and a moderate water-related weakening (f_v <100, Fig. 8). The pre-hydration of the fore-arc mantle is then necessary to model the 580°C isotherm rising up to 20 km depth in less than 40 Myr. In these experiments, the modeled surface heat flux at thinning apex is 67 mW/m^2 at 36.9 Myr, in agreement with the heat flow measured in the Guadeloupe archipelago after having retrieved the radiogenic heat contribution. To conclude, regarding

the range of uncertainties on CPD estimates, our modelling results suggests that to reproduce under realistic thermo-mechanical conditions the present-day CPD doming below the Guadeloupe archipelago, the fore-arc pre-hydration has to be taken into account to simulate an satisfying time of convergence (lower than 40 Ma, maximum duration after the LAA jump).

3.2.2. Subduction conditions in the Saint Barth island area: Influence of convergence rate

Simulations for profile 4 (Fig. 5) are performed with a low convergence rate (1 cm/yr, to model normal convergence in the Northern part of the Lesser Antilles), and with f_v varying from 34.2 to 100 but solely rheology Re. Models include at simulation start the fore-arc mantle pre-hydration computed for the kinematics of profile 4 (Fig. 7c1). The very slow subducting plate dehydrates at shallow depths, yielding a narrow hydration of the arc lithosphere (~28 km wide window, Fig. 7c2). As a result, SSC is strongly delayed and initiates at 91.7 Ma for f_v =50 (simulation SB2, Fig. 7c2). The rising 580°C isotherm reaches the depths of 31 km and 26 km, corresponding to the ones obtained for CPD estimates near Saint Barth island (Fig. 5) very lately, respectively 76.5 Ma and 93 Ma after convergence initiation for f_v=50 (Fig. 8**)**. These times do not significantly vary (84.2 and 92.9 Myr, respectively) when f_v is increased to 100 (Fig. 8). Compared to the Guadeloupe cross-section, the initially pre-hydrated domain in the fore-arc under St Barth island is not only narrower (Fig. 7C1), but is also offset trenchward. Both result in a final hydrated lithosphere that remains quite narrow and prevents an early triggering of arc thinning by SSC. The fore-arc pre-hydration is thus not an efficient accelerating factor of the arc thermal thinning in the case of St Barth profile.

3.2.3. Synthesis on thermo-mechanical experiments

As aforementioned, the simulations show that two major conditions favour a rapid lithosphere thinning independently of horizontal stresses: (1) the fore-arc domain has to be significantly

hydrated before the Oligocene, that is in the northern LAA, where a volcanic arc jump occurred, and (2) the rate of normal convergence must be high enough to enlarge the slab dehydration window sufficiently for SSC to be triggered rapidly. These two conditions are fairly verified from the north of the Martinique to Antigua Island, in agreement with the location and geometry of the main large-scale CPD shallowing. At the Martinique where the ancient and active arcs merge, the CPD rising is likely to result from the upwelling of hot magmas sustaining the intense volcanic activity. At St Barth, normal convergence is too slow to enhance alone the upper lithosphere thinning and the limited width of the initially pre-hydrated domain impedes an early thermo-mechanical thinning of the arc lithosphere.

4. Discussion

4.1. Crustal structure inferred from previous studies at the latitude of the Guadeloupe Island

Our results from two complementary approaches, *i.e.* the CPD determination and the thermo-mechanical modeling, have several fundamental implications on the LAA structure, particularly in the vicinity of the Guadeloupe archipelago. There, the structure of the fore-arc has been extensively studied concerning its deep parts [*Bangs et al.*, 2003; *Christeson et al.*, 2003; *Evain et al.*, 2013; *Kopp et al.*, 2011; *Ruiz et al.*, 2013; *Laigle et al.*, 2013a] and its shallow sedimentary cover [*De Min et al.*, 2015; *Laigle et al.*, 2013b; *Münch et al.*, 2014]. The structure of the LAA crust can be inferred mainly from the combined analysis of wide-angle seismics and pre-stack depth migrated reflection data of *Kopp et al.* [2011]. These authors proposed that the crust of the upper plate beneath the back-arc, the arc and the fore-arc is homogeneous with a rather flat Moho located at 25-28 km depth (Fig. 9a). *Kopp et al.* [2011] distinguished two distinct continuous crustal layers beneath the sedimentary cover: a middle crust, with Vp velocities increasing from 5.5-6.0 to 6.8 km/s, and a lower crust, 12 km thick in average, with Vp velocities increasing from 7.1 to 7.3 km/s. The mantle beneath the Moho would be characterized by P-wave velocities of 8 km/s. This assumed thick crust

extending from the volcanic arc to the fore-arc suggests that the northern-central LAA may rest upon a portion of the Caribbean Oceanic Plateau [*Mauffret and Leroy*, 1997]. However, we evidence a CPD minimum (18.5 km) in the inner fore-arc domain suggesting a doming of magnetic sources. On one hand, this could suggest a strong petrological change within the lower crust but such a change is not consistent with the homogeneous velocity of the lower crust proposed by *Kopp et al.* [2011]. Keeping in mind the overall uncertainty of about 5 km on our CPD estimation (due to possible fractal behavior of magnetization, dataset resolution, window size), our results question the crustal structure proposed by *Kopp et al.* [2011].

Moreover, such a thick homogeneous crust is inconsistent with long-wavelength gravity anomalies [*Gailler et al.*, 2013] (Fig. 9b). In the inner fore-arc, two main along-arc gravity anomalies were documented, a negative signal close to the active arc and a positive one close to the outer-arc. The main negative anomaly has been associated with two main subsident areas: the first one is parallel to the arc and the second one is oriented N130° following the Tiburon oceanic ridge direction. The main positive anomaly is clearly related to basement highs, since the basement is outcropping at La Désirade and at the Karukéra spur. Inversely, long-wavelength magnetic anomalies are strongly positive in the inner fore-arc, between the ancient and active arcs, and negative close to the outer fore-arc (Fig. 9b). Such geometry and spatial offset between long-wavelength gravity and magnetic anomalies have already been observed in the Cascadia subduction zone and interpreted as the signature of a low density and highly magnetized serpentinized mantle wedge [*Bostock et al.*, 2002; *Blakely et al.*, 2005]. *Arnaiz-Rodriguez and Orihuela* [2013] proposed that the observed magnetic anomaly in northern-central LAA was related to the occurrence of a well-developed mantle wedge beneath the fore-arc, which disagrees with *Kopp et al.*'s [2011] model. We have tested this hypothesis with a simultaneous gravity and magnetic 2D forward model along the seismic profile (Fig. 9b). As underlined by *Blakely et al.* [2005], serpentinite are low in density while

having very high magnetization. Serpentinization tends to decrease the density of peridotite from $3x10^3$ $kg.m^{-3}$ to $2.5x10^3$ $kg.m^{-3}$ [*Christensen*, 1966; *Saad*, 1969]. Furthermore, serpentinization produces magnetite, increasing remanent magnetization by at least one order of magnitude [*Saad*, 1969]. Accordingly, the serpentinized mantle is assigned a density of $2.8x10^3$ $kg.m^{-3}$ and a magnetization of 1.4 $A.m^{-1}$ on the basis of rock-magnetic studies of ultramafic rocks [*Saad*, 1969]. Other lithologies are assigned densities and magnetizations derived from the seismic profile from *Kopp et al.* [2011] using the relation defined by Gebrande et al. [1982] and adjusted according to published values [*Christenson et al.*, 2008; Tab. 2]. As evidenced on Figure 9b, the density model without serpentinized mantle leads to an anomaly higher in amplitude compared to the observations. Considering a low or non-magnetization below the middle crust interpreted from Kopp et al. [2011] does not allow satisfying the amplitude of the observed magnetic anomaly. A serpentinized mantle, low in density while having very high magnetization is therefore required to satisfy the amplitude of both magnetic and gravity anomaly. In detail, the discrepancies between observed and modeled data are reliable to the fact that we focus on the regional deep sources without studying the local shallow structures.

Eventually, *De Min et al.* [2015] showed that the inner fore-arc at the latitude of the Guadeloupe archipelago is subsident since the late Paleogene–early Miocene, consistently with the negative gravimetric anomaly [*Gailler et al.*, 2013]. This subsidence was related to four main extensional tectonic episodes since the early Miocene with various directions of extension. According to *De Min et al.* [2015], such configuration and tectonic regime of the central Lesser Antilles fore-arc domain suggest that the subduction is erosive in this part of the LAA. Therefore the extensional and subsiding setting of the inner fore-arc basin since at least ~30 Ma is inconsistent with the assumed homogeneous crustal thickness of *Kopp et al.* [2011].

4.2. Hypothesis of a serpentinized mantle wedge

The thermo-mechanical modeling of the Guadeloupean subduction segment developed here shows that slab dehydration triggers the fore-arc mantle serpentinization (Fig. 7). Besides, simulations show that a pre-hydration of the mantle wedge promotes a rapid serpentinization after the volcanic arc jump, as well as a faster heating of the upper lithosphere. At final stages of simulations, i.e. when the 580°C isotherm has reached either the 25 km or the 20 km depths, models predict the formation of a serpentinite layer, with a percentage of serpentine of at most 40% in volume, at depth shallower than the ~600°C isotherm. As magnetite is a by-product of mantle serpentinization [*Saad*, 1969], our modeling argues that the high magnetic anomaly detected all along the double arc in the northern-central LAA (Fig. 2) might witness the mantle wedge serpentinization, as proposed for the Cascadia subduction zone [*Bostock et al.*, 2002; *Blakely et al.*, 2005]. At first order, this result is in contradiction with the model of *Kopp et al.* [2011] assuming that P-wave velocity within the overriding lithospheric mantle is 8 km/s, corresponding thus to an anhydrous mantle. Serpentinization strongly decreases seismic bulk Vp velocity, from 8.4 to 7 km/s for 0 to 40% serpentinization [*Christensen*, 1966; *Hyndman and Peacock*, 2003]. As a consequence, we propose that the seismic layer where Vp increases from 7.1 to 7.3 km/s in the model of *Kopp et al.* [2011] corresponds to a serpentinized mantle layer rather than to a lower crustal level. Indeed, Vp velocities between 7.1 and 7.3 km/s may correspond to 32-38% of serpentinization [*Christensen*, 1966; *Hyndman and Peacock*, 2003], in good agreement with our simulations.

4.3. New model for the northern-central LAA structure

The structure of the northern-central LAA is therefore refined using our high-resolution CPD calculations to complement seismic imaging. Near the Guadeloupe Island, our re-interpretation of the lower part of the seismic tomography profile by *Kopp et al.* [2011] leads to a much shallower and irregular Moho beneath the inner fore-arc (i.e. close to the ancient

arc) located at a minima depth of ~13 km (Fig. 9c). Even if our study cannot provide exact geometry of the Moho, the location where we predict the Moho to be the shallowest is close to the one of the CPD minima recognized in the inner fore-arc. We propose this geometry to be the result of an intense thermal thinning in this area, as modeled in our thermo-mechanical experiments, when a pre-hydrated mantle wedge simulates the influence of an ancient arc. Our proposition is in agreement with 1) the extensive tectonics, lasting since at least ~35 Ma, and the subsidence of the inner fore-arc basin, evidenced by *De Min et al.* [2015], 2) the a long-axis negative gravimetric anomaly compatible with the extensional environment [*Gailler et al.*, 2013], 3) magnetic anomalies in the fore-arc, and 4) the lack of thrust earthquakes in the Guadeloupe fore-arc [*Laigle et al.*, 2013a]. Moreover, the assumed Curie temperature for magnetite (580°C) is close to the upper temperature of stability of serpentine [*Schmidt and Poli*, 1998]. Therefore, if the magnetic signal detected in the LAA fore-arc mainly comes from mantle magnetite derived from serpentinization, then the CPD might roughly correspond to the base of the serpentinized mantle (Fig. 9c). The main consequences of the fore-arc structure beneath the Guadeloupe archipelago evidenced in this paper are the followings:

- The seismic discontinuity between 7.3 and 8 km/s, located at ~28 km depth and interpreted as the Moho in *Kopp et al.* [2011], may correspond to a lithological contrast within the mantle wedge, for instance to an hydration front. Nonetheless, this deep interface is not very well constrained in the model proposed by *Kopp et al.* [2011] (Fig. 9c).

- The seismicity observed below 15 km depth in the Guadeloupe fore-arc is likely to mainly occur within the inner fore-arc mantle wedge, such as in the Martinique fore-arc [*Laigle et al.*, 2013a, *Ruiz et al.*, 2013]. As the Guadeloupe fore-arc mantle is assumed to be serpentinized, this seismicity pattern is also similar to the one described in northeast New Zealand [*Davey et al.*, 2011], in southern Japan [*Miura et al.*, 2003] and in northeastern Japan [*Uchida et al.*,

2010]. In northeast New Zealand and southern Japan, a low P velocity (7 < Vp < 8 km/s) serpentinized mantle has been identified beneath the fore-arc and it is the locus of numerous earthquakes. Moreover, *Davey et al.* [2011] show that this seismicity is probably mainly located near the interface between a dry mantle and a serpentinized mantle. In the Guadeloupe fore-arc mantle, earthquakes would also occur near the hydration front in the proposed model (Fig 9c). The origin of this intra mantle wedge seismicity is still a matter of debate, as serpentinite is thought to be aseismic [*Kirby et al.*, 1996]. Dehydration embrittlement [*e.g. Davey et al.*, 2011] or seamounts detached from the slab [*Uchida et al.*, 2010] could be evoked, but a detailed discussion dealing with this issue is beyond the scope of this paper.

- The downdip extent of the fore-arc crust/subducted plate interface may be significantly reduced considering a Moho shallower than in *Kopp et al.*'s [2011] model (Fig. 9c). The serpentinized mantle, immediately beneath the arc crust Moho, would occur at the hangingwall of the subduction interface, implying a possibly weaker seismic coupling along the subduction plane. This is in agreement with the lack of earthquake in this domain (Fig. 9c) that has also been related to the subduction of sediments beneath the backstop [*Christeson et al.*, 2003]. This is moreover consistent with basal erosion processes, suggested by *Münch et al.* [2014] and *De Min et al.* [2015], rather than with frontal accretion. Indeed, *Bangs et al.* [2003] proposed that half of the sediments underthrusted at the toe of the accretionary wedge may be subducted down to 15 km beneath the backstop/outer fore-arc.

In the northern LAA, near St Barth Island, an important positive magnetic anomaly is also observed but it is associated only with secondary domings of the CPD and to a slight CPD deepening beneath the ancient volcanic arc (Fig. 4a). Even if the thermo-mechanical model (profile 4; Fig. 7) predicts the formation of serpentinite at shallow depth, it does not simulate an early thermal thinning of the fore-arc lithosphere, precluding a rapid (<40 Ma) shallowing

of isotherms as in the Guadeloupe inner fore-arc, essentially because the lateral extent of fore-arc serpentinization is stronly limited by the very low convergence rate. Thus, the structure of the fore-arc, as well as the subduction interplate conditions, in the vicinity of St Barth island must be very different from the ones in the Guadeloupe area, mainly because of a slower normal convergence rate in the northern LAA. As the deep structure of the subduction zone remains not accurately defined there, the degree of interplate coupling cannot be inferred.

5. Conclusions

In this work, we address the thermal structure of the northern LAA subduction by combining a Curie Point Depth computation from magnetic spectral analysis, and a thermo-mechanical modeling. Even regarding the overall uncertainty of our CPD estimates, we evidence an anomalous main CPD doming, both in amplitude (CPD rises up to ~18.5 km depth) and wavelength, in the inner fore-arc domain at the latitude of the Guadeloupe archipelago and more or less below the ancient and inactive arc. This doming corresponds to a positive long-wavelength magnetic anomaly in the fore-arc domain and suggests a particularly hot thermal state in this part of the fore-arc domain where no heat flow measurement is available.

We use 2D thermo-mechanical simulations to discuss the parameters controlling such a fore-arc thermal structure and we take into account the ~35 Ma volcanic arc jump that occurred in the northern LAA. To simulate the present-day Guadeloupe thermal state deduced from CPD estimates, we find that: (1) the dry mantle ductile strength has to be relatively low; (2) the amplitude of the modeled water-related weakening must be high enough (≥50); and (3) a pre-hydration of the fore-arc mantle, simulating the effect of the ancient arc before arc jump, is required in most cases as a efficient factor of fast arc thinning. In all experiments, we predict a significant serpentinization of the mantle wedge (~35% in volume over a 28 to 80 km width). As magnetite is a by-product of mantle serpentinization, our results are consistent with the positive magnetic anomaly observed along the double (ancient and active) arc.

Consequently, we propose a new model for the crustal structure of the Guadeloupe fore-arc from the re-interpretation of a published seismic velocity profile below the Guadeloupe archipelago [*Kopp et al.,* 2011]. We propose that the seismic layer characterized by Vp varying from 7.1 to 7.3 km/s, previously interpreted by *Kopp et al.* [2011] as the lower crust of the fore-arc, may rather be a layer of serpentinized mantle, compatible with Vp velocities

predicted for a ~35% serpentinized peridotite [Christensen, 1966; Hyndman and Peacock, 2003]. Our hypothesis is supported by gravimetric and magnetic anomalies and their relative spatial locations [*Gailler et al.*, 2013]. This pattern is comparable to the one observed in the Cascadia subduction zone which was interpreted as the signature of a strong mantle wedge serpentinization [*Blakely et al.*, 2005]. Moreover our hypothesis of a crustal thinning of the Guadeloupe inner fore-arc is in agreement with the long lasting (*i.e.* since Oligocene) extensional tectonics and subsidence history evidenced in this domain by *De Min et al.* [2015]. Accordingly, we propose to re-interpret the seismic interface across which Vp jumps from 7.3 km/s to 8 km/s, interpreted as the Moho in *Kopp et al.* [2011], as a front of mantle hydration.

Finally, our re-interpretation implying a shallow fore-arc serpentinization in the vicinity of the subduction interface argue, on one hand, for the seismicity to be mainly located in the mantle wedge, and, on the other hand, for a low interplate coupling of the Lesser Antilles subduction interface at the latitude of Guadeloupe. We have to keep in mind that the proposed mechanism of CPD shallowing is consistent with Guadeloupe setting but cannot explain the less pronounced minima elsewhere along the arc. Further to the north, this structure cannot be extended with confidence, because we lack seismic imaging of the subduction zone in this part. Despite the reduced normal rate of convergence northwards, our results however predict a serpentinized mantle wedge there.

Acknowledgments

This research was financed by the French Government Laboratory of Excellence initiative, the Région Auvergne and the European Regional Development Fund. This work has benefited from data acquired by numerous scientific projects. We thank the NOAA and Stephen Maus for the diffusion of the global relief model of Earth's surface, and Earth's magnetic database respectively. We are also grateful to Richard J. Blakely, Serge Lallemand, Jean-Jacques Cornée, for their contribution and discussions about this study. Stéphane Arnal, Fabrice Grosbeau, and Josiane Tack are acknowledged for the maintenance and development of the cluster of computing nodes on which all numerical experiments were performed. The manuscript greatly benefited from the comments and reviews from Jeroen van Hunen, Marc-André Gutcher and three anonymous reviewers.

Table Captions

Table 1: CPD and Moho depth comparison in the study area.

Table 2: Physical properties used in gravity and magnetic models (Fig. 9b).

Figure Captions

Figure 1: Large scale context of the LAA (after [*Bouysse and Westercamp*, 1988]).

Figure 2: Magnetic anomaly map computed at 4 km a.s.l. (cell size 470 m) from the compilation of the aeromagnetic survey [*LeBorgne and LeMouel*, 1976] marine dataset [*Gailler et al.*, 2013] and EMAG-V2 [*Maus*, 2009]. The location of the various datasets is shown in the right-bottom side. The black solid contours refer to the 0 m isobaths. The black crosses locate the center of each CPD computation window (120 x 120 km; Fig. 3). The underlying shaded large scale bathymetry is extracted from ETOPO model (1 arc-minute global relief model of Earth's surface that integrates land topography and ocean bathymetry) available from the NOAA database at http://www.ngdc.noaa.gov/mgg/global/global.html). Coordinates in kilometers (WGS84, UTM 20N).

Figure 3: Example of azimuthally averaged power spectra for the estimation of the depth to the magnetic bottom using the two-dimensional upward continued magnetic anomaly data (data covering the 120x120 km subregion centered on 638.125-1782.890 km, located on top). According to Tanaka et al. (1999), z_0 and zt are defined as the centroid and the top bound of the magnetic sources respectively (|k| is the wavenumber and $\phi_{\Delta T}$ (|k|) is the spectrum of the magnetic anomaly). The main slopes and the noise level are underlined on each graph.

Figure 4: a) Calculated CPD map represented by both color-coded square windows and interpolated contours. The main structural features are located. Heat flow measurements are located by stars [*Manga et al.*, 2012]. **b)** Map of the misfit (eq. 3) between the theoretical curve and the radial power spectra (Fig. 3). For the calculation of the theoretical curve (eq. 2), we used the estimated values of z_t and $\Delta z = z_b - z_t$. For the entire area,the root-mean-square (RMS) of the misfit value is equal to 0.92. **c)** Depth to Moho relative to sea level are extracted from Crust1.0 model [*Laske et al.*, 2013]. Coordinates in kilometers (WGS84, UTM 20N).

Figure 5: Comparison between CPD estimates and bathymetry along four main profiles of interest located in the CPD map on top.

Figure 6: a) Geometry of the simulation box and boundary conditions. The inserted black box represents both the region where the numerical mesh is refined and the close-up displayed in panels b and c. **Panels b and c :** Simulated rheologies (labels «Re» and « St ») versus experimentally determined rheologies for crustal compositions (a) and mantle rocks (b). Stress profiles are computed for a 100 km thick lithosphere geotherm and a uniform reference strain rate equal to 10^{-14} s^{-1}. « R&M87 »: *Ranally and Murphy* [1987]; «K83 »: *Kirby* [1983]; «W&C90» : *Wilks and Carter* [1990]; «G&T95»: *Gleason and Tullis* [1995]; «E&K95»: *Evans and Kohlstedt* [1995]; «H&K96»: *Hirth and Kohlstedt* [1996]; «C&P81»: *Chopra and Paterson* [1981]; «Kal86»: *Karato et al.* [1986]. **Panel d**: Modeled strength reduction for the ductile mantle as a function of water content. The water content scale is displayed in mol/m^3, but corresponding values in weight percent are indicated. amph : stable amphibole; chl : stable chlorite; serp: stable serpentine. Colors refer to the color scale of water content used in panel a.

Figure 7: Panels a1-4: Simulation G4 with a 2 cm/yr convergence rate when no hydration is imposed in the upper plate at convergence start (rheology Re and f_v=50). **Panels b1-4**: Simulation G5 with a 2 cm/yr convergence rate and an initial water-saturation in the fore-arc domain at convergence start (rheology Re and f_v=50). **Panels c1-2**: Simulation SB5 with a 1 cm/yr convergence rate and an initial fore-arc hydration at convergence start (rheology Re and f_v=50). Isotherms (white lines) are depicted every 200°C. The pink line is the 580°C isotherm. The black outline delimits the subducting 'crustal' layer. Blue arrows indicate the location of the shallowest depth of the 580°C isotherm. «T » : trench location.

Figure 8: Characteristic times of fore-arc lithosphere heating, measured as the duration of convergence necessary to model the 580°C isotherm shallowing within the overriding lithosphere up to either 20 km depth (profile 3 modeling, 2 cm/yr) or 26 km (profil 4 modeling, 1 cm/yr), as a function of the maximum amount of water-related weakening, $f_{\square}$. 'FA pre-hydr': Fore-arc pre-hydration imposed at simulation initiation. 'No pre-hydr': No pre-hydration of the fore-arc mantle imposed at convergence start.

Figure 9: a) 2D velocity model across the Lesser Antilles island arc [*Kopp et al.*, 2011]. The dashed blue line underlines the upper bound of the low resolution of the seismic rays (bleached downward). **b)** Simultaneous gravity and magnetic model along the 2D velocity model. Upper panel: thick lines labeled 'serpentinized mantle alone' refer to gravity and magnetic response of a serpentinized crust alone. Dashed lines refer to models considering a CPD 5km deeper, corresponding to the overall uncertainty on our estimation. Lower panel: dotted areas locate the paramagnetic layers. See Table 3 for physical properties used in model (ρ: density in 10^3 kg.m^{-3}; A: magnetization in A.m^{-1}). The magnetic profile is extracted from the map presented in this study. The gravity profile is extracted from the gravity map computed by *Gailler et al.* [2013]; **c)** New interpretation along the seismic profile from *Kopp et al.* [2011] derived from this study and the recent geological considerations from *De Min et al.* [2015] and *Münch et al.* [2014].

References

Andreieff, P., Bouysse, P., Westercamp, D., 1989. Géologie de l'arc insulaire des Petites Antilles et évolution géodynamique de l'Est-caraïbe. Bordeaux I.

Arnaiz-Rodríguez, M.S., Orihuela, N., 2013. Curie point depth in Venezuela and the Eastern Caribbean. Tectonophysics 590, 38–51. doi:10.1016/j.tecto.2013.01.004

Ates, A., Bilim, F. and Buyuksarac, A., 2005. Curie point depth investigation of Central Anatolia, Turkey. Pure appl. Geophys. 162, 357–371.

Arcay , D., Tric, E., Doin, M.-P., 2005. Numerical simulations of subduction zones: Effect of slab dehydration on the mantle wedge dynamics, Phys. Earth Planet. Int., 149, 133-153.

Arcay , D., Doin M.-P., Tric, E., Bousquet, R., de Capitani, C., 2006. Overriding plate thinning in subduction zones: Localized convection induced by slab dehydration, Geochem. Geophys. Geosyst., 7, doi :10.1029/2005GC001061, Q02007.

Arcay , D., Lallemand, S., Doin M.-P., 2008. Back-arc Strain in Subduction Zones: Statistical Observations vs. Numerical Modelling, Geochem. Geophys. Geosyst., 9, doi :10.1029/2007GC001875, Q05015.

Arcay , D., 2012. Dynamics of interplate domain in subduction zones: influence of rheological parameters and subducting plate age, Solid Earth, 3, 467-488, doi: 10.5194/se-3-467-2012, http://www.solid-earth.net/3/467/2012/.

Arcay, D., 2017. Modelling the interplate domain in thermo-mechanical simulations of subduction: Critical effects of resolution and rheology, and consequences on wet mantle melting. Physics of the Earth and Planetary Interiors, in revision.

Bhattacharyya, B.K., Leu, L.-K., 1975a. Spectral analysis of gravity and magnetic anomalies due to two-dimensional structures. Geophysics 40, 993–1013.

Bhattacharyya, B.K., Leu, L.-K., 1975b. Analysis of magnetic anomalies over Yellowstone National Park: mapping of Curie point isothermal surface for geothermal reconnaissance. Geophys. Res. Lett. 80, 4461–4465.

Bijwaard H., 1999. Seismic travel-time tomography for detailed global mantle structure, PhD thesis, Utrecht University, 181, 178pp.

Blakely, R.J., 1988. Curie temperature isotherm analysis and tectonic implications of aeromagnetic data from Nevada. J. Geophys. Res. 93, 11,817– 11,832.

Blakely, R.J., Brocher T.M., Wells R.E., 2005. Subduction-zone magnetic anomalies and implications for hydrated forearc mantle, Geology; June 2005; v. 33; no. 6; p. 445–448; doi: 10.1130/G21447.1

Boioli, F., Tommasi, A., Cordier, P., Demouchy, S., Mussi, A., 2015. Low steady-state stresses in the cold lithospheric mantle inferred from dislocation dynamics models of dislocation creep in olivine, Earth and Planetary Science Letters, 232–242.

Bostock, M.G., Hyndman, R.D., Rondenay, S., and Peacock, S.M., 2002, An inverted continental Moho and serpentinization of the forearc mantle: Nature, v. 417, p. 536–538.

Bouligand, C., Glen, J.M.G., Blakely, R.J., 2009. Mapping Curie temperature depth in the western United States with a fractal model for crustal magnetization. J Geophy Res 114: 1–25.

Bousquet, R., Goffé, B., Henry, P., Le Pichon, X., Chopin, C., 1997. Kinematic, thermal and petrological model of the Central Alps: Lepontine metamorphism in the upper crust and eclogitisation of the lower crust, Tectonophysics, 273, 105-127.

Bouysse, P., 1979. Caractères morphostructuraux et évolution géodynamique de l'arc insulaire des Petites Antilles (Campagne Arcante1). Orléans.

Bouysse, P., Westercamp, D., 1988. Effets de la subduction de rides ocaéaniques sur l'évolution d'un arc insulaire: l'exemple des Petites Antilles, Géologie de la France, n°2-3, pp 3-36.

Boynton, C. H., Westbrook, G. K., Bott, M. H. P., Long, R. E., 1979. A seismic refraction investigation of crustal structure beneath the Lesser-Antilles island arc, Geophys. J. R. Astron. Soc., 58, 371–393.

Briden, J.C., Rex, D.C., Fallar, A.M. and Tomblin, J.F., 1979. K–Ar geochronology and palaeomagnetism of volcanic rocks from the Lesser Antilles Island Arc. Philos. Trans. R. Soc. Lond. Ser. A Math. Phys. Sci. 291, 485–528.

Bunce, E.T., Phillips, J.D., Chase, R.L., et al., 1971. The Lesser Antilles arc and the eastern margin of the Caribbean sea, in: Maxwell, A.E. (Ed.), The Sea, Vol. 4. New York, pp. 359–385.

Campos-Enriquez, J.O., Arroyo-Esquivel, M.A., Urrutia-Fucugauchi, J., 1990. Basement, Curie isotherm and shallow-crustal structure of the Trans-Mexican Volcanic Belt, from aeromagnetic data. Tectonophysics 172, 77–90.

Campos-Enriquez, J.O., Urrutia-Fucugauchi, J., Arroyo-Esquivel, M.A., 1989. Depth estimations to the Curie isotherm from aeromagnetic data and geothermal considerations for the western sector of the Trans-Mexican Volcanic Belt. Geofis. Int. 28, 993–1005.

Chopra, P.N., and Paterson, M.S., (1981) The experimental deformation of dunite. Tectonophysics 78: 453–473.

Christensen, N.I., 1966. Elasticity of ultrabasic rocks, J. Geophys. Res., 71, 5921-5931.

Christensen, U., Yuen, D.A., 1984. The interaction of a subducting lithosphere slab with a chemical of phase boundary, J. Geophys. Res., 89, 4389-4402.

Christensen, U., 1992. An Eulerian technique for thermomechanical modeling, J. Geophys. Res., 97, 2015-2036.

Christeson, G.L., Bangs, N.L., Shipley, T.H., 2003. Deep structure of an island arc backstop, Lesser Antilles subduction zone. J. Geophys. Res. 108, 2327, doi:10.1029/2002JB002243.

Christeson, G.L., Mann, P., Escalona, A., et al., 2008. Crustal structure of the Caribbean–northeastern South America arc-continent collision zone. J. Geophys. Res. 113, B08104. doi:10.1029/2007JB005373

Clark, T.F., Korgen, B.J., Best, D.M., 1978. Heat flow in the eastern Caribbean. J. Geophys. Res. 83, 5883. doi:10.1029/JB083iB12p05883

Connard, G., Couch, R., Gemperle, D. l. F., 1983. Analysis of aeromagnetic measurements from the Cascade Range in central Oregon. Geophysics 48, 376–390.

Davey, F.J., Ristau, J., 2011. Fore-arc mantle wedge seismicity under northeast New Zealand, Tectonophysics, 509, 272-279, doi:10.1016/j.tecto.2011.06.017.

Davis, D.M., Hussong, D.M., 1983. Geothermal observations during Deep Sea Drilling Project LEG 78A. Initial Reports of the Deep Sea Drilling Project 78A.

DeMets, C., Jansma, P., Mattioli, G., et al., 2000. GPS Geodetic constraints on Caribbean-North American plate motion. Geophys. Res. Lett. 27, 437–440.

De Min L., Lebrun J.-F., Cornee J.-J., Münch Ph., Leticee J.-L., Quillevere F., Melinte-Dobrinescu M., Randrianasolo A., Marcaillou B., Zami F., and the KaShallow team, 2015. Tectonic and sedimentary architecture of the Karukéra spur: A record of the Lesser Antilles fore-arc deformations since the Neogene. Mar. Geol. 363, 15-37. doi.org/10.1016/j.margeo.2015.02.007.

Demouchy, S., Tommasi, A., Boffa-Ballaran, T., Cordier, P., 2013. Low strength of Earth's uppermost mantle inferred from tri-axial deformation experiements on a anhydrous olivine crystals. Phys. Earth Planet. Int., 220, 37-49, doi:10.1016/j.pepi.2013.04.008.

Deng, J., Sykes, L.R., 1995. Determination of Euler pole for contemporary relative motion of Caribbean and NWrth American plates using slip vectors of inter-plate earthquakes. Tectonics 14, 39–53.

De Ritis, R., Ravat, D., Ventura, G., Chiappini, M., 2013. Curie isotherm depth from aeromagnetic shallow heat source depths in the Southern Tyrrhenian Sea, Italy, Bull Volcanol 75:710, DOI 10.1007/s00445-013-0710-9.

Diebold, J., 2009. Submarine volcanic stratigraphy and the Caribbean LIP's environment. Geol. Soc. London Spec. Pub. 328, 799–808.

Dixon, T., Farina, F., DeMets, C., et al., 1998. Relative motion between the Caribbean and North American plates and related boundary zone deformation based on a decade of GPS observations. J. Geophys. Res. 103, 15157–15182.

Dumoulin, C., Doin, M.-P., Fleitout, L., 2001. Numerical simulations of the cooling of an oceanic litosphere above a convective mantle, Phys. Earth Planet. Int., 125, 45-64.

Dyment, J., Arkani-Hamed, J., and Ghods, A., 1997. Contribution of serpentinized ultramafics to marine magnetic anomalies at slow and intermediate spreading centres: insights from the shape of the anomalie, Geophysical Journal International 129.3, 691-701.

Epp, D., Grim, P.J., Langseth, M.G., 1970. Heat flow in the Caribbean and Gulf of Mexico. J. Geophys. Res. 75, 5655–5669.

Evain, M., Galve, A., Charvis, P., Laigle, M., Kopp, H., Bécel, A., Weinzierl, W., Hirn, A., Flueh, E.R., Gallart, J. and the Lesser Antilles Thales scientific party, 2013. Structure of

the Lesser Antilles subduction forearc and backstop from 3D seismic refraction tomography, Tectonophysics, 603, 55-67, doi:10.1016/j.tecto.2011.09.021.

Evans, B., and Kohlstedt, D.L. (1995) Rheology of rocks. In: Ahrens TJ (ed.) AGU Reference Shelf 1: Rock Physics and Phase Relations: A Handbook of Physical Constants, pp. 149–165. Washington, DC.

Fedi, M.., 2016. Scaling Laws in Geophysics: Application to Potential Fields of Methods Based on the Laws of Self-similarity and Homogeneity. In 'Fractal solutions for understanding complex systems in Earth sciences', Ed. V. P. Dimri, Springer.

Fedi, M., Quarta, T., De Santis, A., 1997. Inherent power-law behavior of magnetic field power spectra from a Spector and Grant ensemble. Geophysics, 62(4), 1143-1150.

Fernández, D., 2004. Análisis de la Cuenca Oriental de Venezuela a partir de informacion de pozos. Simon Bolivar, Caracas.

Ferré, E.C., Friedman, S.A., Martín-Hernández, F., et al., 2014. Eight good reasons why the uppermost mantle could be magnetic. Tectonophysics 624-625, 3–14.

Feuillet, N., 2002. Arc parallel extension and localization of volcanic complexes in Guadeloupe, Lesser Antilles. J. Geophys. Res. 107, 2331. doi:10.1029/2001JB000308

Feuillet, N., Leclerc, F., Tapponnier, P., et al., 2010. Active faulting induced by slip partitioning in Montserrat and link with volcanic activity: New insights from the 2009 GWADASEIS marine cruise data. Geophys. Res. Lett. 37, n/a–n/a. doi:10.1029/2010GL042556

Fleitout, L., Yuen, D., 1984. Secondary convection and the growth of oceanic lithosphere, Phys. Earth Planet. Int., 36, 181-212.

Fox, P.J., 1971. The geology of the Caribbean crust: tertiary sediments, and basic rocks from the Aves Ridge. Tectonophysics 12, 89–109.

Gailler, L.S., Lénat, J.F., Blakely, R.J., 2016. Depth to Curie temperature or magnetic sources bottom in the volcanic zone of La Réunion hot spot. Journal of Volcanological and Geothermal Research, 324, p 169-178, doi:10.1016/j.jvolgeores.2016.06.005.

Gailler, L.S., Martelet, G., Thinon, I., Bouchot, V., Lebrun, J.-F., Münch, Ph., 2013. Crustal structure of Guadeloupe islands and the Lesser Antilles arc from a new gravity and magnetic synthesis. Bull. la Soc. Geol. Fr. 184, 77–97.

Gettings, M. E., 2005. Multifractal magnetic susceptibility distribution models of hydrothermally altered rocks in the Needle Creek Igneous Center of the Absaroka Mountains, Wyoming, Nonlinear Processes Geophys., 12, 587– 601.

Gleason, G.C., and Tullis, J. (1995) A flow law for dislocation creep of quartz aggregates determined with the molten salt cell. Tectonophysics 247: 1–23.

Gripp, A. E., and R. G. Gordon (2002), Young tracks of hot- spots and current plate velocities, Geophys. J. Int., 150, 321 – 361.

Gutscher, M.A., Westbrook, W.K.., Marcaillou, B., Graindorge, D., Gailler, A., Pichot, T., Maury, R.C., 2013. How wide is the seismogenic zone of the Lesser Antilles forearc? In :J.F.Lebrun and B. Marcaillou, Eds, Caribbean geosciences. – Bull. Soc. géol. Fr., 184,1.

Hernández, M., 2006. Modelado numérico termal 1D de la Cuenca Oriental de Venezuela. Simon Bolivar, Caracas.

Hirth, G., and Kohlstedt, D.L. (1996) Water in the oceanic upper mantle: Implications for rheology, melt extraction and the evolution of the lithosphere. Earth and Planetary Science Letters 144: 93–108.

Holbrook, W.S., Lizarralde, D., McGeary, S., et al., 1999. Structure and composition of the Aleutian island arc and implications for continental crustal growth. Geology 27, 31–34.

Hyndman, R.D., Peacock, S.M., 2003. Serpentinization of the forearc mantle, Earth Planet. Sci. Lett., 212, 417-432.

Karato, S.-I., Paterson, M.S., and FitzGerald, J.D., 1986. Rheology of synthetic olivine aggregates: Influence of the grain size and water. Journal of Geophysical Research 91: 8151–8176.

Kelemen, P.B., Rilling J.L., Parmentier E.M., Mehl, L., Hacker, B. R., Thermal structure due to solid-state flow in the mantle wedge beneath arcs, 2003. In "Inside the Subduction factory", John Eiler (Ed.), Geophys. Monogr. Ser., 138, 293-311, AGU, Washington D.C

Kearey, P., 1976. Gravity and seismic reflection investigation into the crustal structure of the Aves Ridge, eastern Caribbean, in: Trans. 7th Caribbean Geol. Conf. Guadeloupe, pp. 311–320.

Kirby, S.H. (1983) Rheology of the lithosphere. Reviews of Geophysics 21: 1458–1487.

Kirby, S., Engdahl, E.R., Denlinger R., 1996. Intermediate-depth intraslab earthquakes and arc volcanism as physical expressions of crustal and uppermost mantle metamorphism in subducting slabs, in "Subduction: Top to bottom", Gray E. Bebout, David W. Scholl, Stephen H. Kirby and John P. Platt (ed.), Geophys. Monogr. Ser. vol. 96, 195-211, AGU, Washington D.C.

Kopp, H., Weinzierl, W., Becel, a., et al., 2011. Deep structure of the central Lesser Antilles Island Arc: Relevance for the formation of continental crust. Earth Planet. Sci. Lett. 304, 121–134. doi:10.1016/j.epsl.2011.01.024

Laigle, M., et al., 2005. Elements of the seismic structure and activity of the Lesser Antilles SISMANTILLES, subduction zone (Guadeloupe and Martinique Islands) from the seismic survey. Eos Trans. AGU 86 (52), T33C-0580 Fall Meet. Suppl., Abstr.

Langseth, M.G., and P.J. Grim (1964), New heat-flow measurements in the Caribbean and western Atlantic, J. Geophys. Res., 69, 4916–4917, doi:10.1029/JZ069i022p04916.

Langseth, M.G., Von Herzen, R.P., 1970. Heat flow through the floors of the world oceans, in: Maxwell, A.E. (Ed.), The Sea, 4. pp. 299–352 (780).

Laske, G., Masters., G., Ma, Z. and Pasyanos, M., 2013. Update on CRUST1.0 - A 1-degree Global Model of Earth's Crust, Geophys. Res. Abstracts, 15, Abstract EGU2013-2658.

LeBorgne, E., LeMouël, J.L., 1976. Le levé aéromagnétiques des Antilles françaises, observations magnétiques. Publ. IPGP, n°26, 25 p. J. Geophys. Res. 79, 324.

Li, C.F., Shi, X., Zhou, Z., Li, J., Geng, J. and Chen, B., 2010. Depths to the magnetic layer bottom in the South China Sea area and their tectonic implications. Geophys. J. Int. 182, 1229–1247 doi: 10.1111/j.1365-246X.2010.04702.

Li, C.F., Wang, J., Zhou, Z., Geng, K., Chen, B., Yang, F., Wu J., Yu, P., Zhang, X., Zhang, S., 2012. 3D geophysical characterization of the Sulu–Dabie orogen and its environs. Physics of the Earth and Planetary Interiors 192–193 (2012) 35–53 doi:10.1016/j.pepi.2012.01.003.

Li, C.F., Wang, J., Lin, J., Wang. T., 2013. Thermal evolution of the North Atlantic lithosphere: new constraints from magnetic anomaly inversion with a fractal magnetization model. Geochemistry Geophysics Geosystems 14: 5078–5105.

Lovejoy, S., Pecknold, S., and Schertzer, D., 2001. Stratified multifractal magnetization and surface geomagnetic fields-I. Spectral analysis and modelling, Geophys. J. Int., 145, 112 – 126, doi:10.1111/j.1365-246X. 2001.00344.x.

Manea, M. and Manea, V.C., 2011. Curie Point Depth Estimates and Correlation with Subduction in Mexico. Pure Appl. Geophys. 168: 1489. doi:10.1007/s00024-010-0238-2.

Manga, M., et al., 2012. Heat flow in the Lesser Antilles island arc and adjacent back arc Grenada basin, Geochem. Geophys. Geosyst., 13, Q08007, doi:10.1029/2012GC004260.

Marlowe, J.J., 1968. Geological reconnaissance of parts of Aves Ridge, in: Fifth Caribbean Geological Conference. Puerto rico, pp. 51–52.

Mauffret, A., Leroy, S., 1997. Seismic stratigraphy and structure of the Caribbean igneous province. Tectonophysics 283, 61–104.

Maus, S., and Dimri, V. P., 1995. Potential field power spectrum inversion for scaling geology, J. Geophys. Res., 100, 12,605–12,616, doi:10.1029/ 95JB00758.

Maus, S., and Dimri, V. P., 1996. Depth estimation from the scaling power spectrum of potential fields?, Geophys. J. Int., 124, 113 – 120, doi:10.1111/j.1365-246X.1996.tb06356.x.

Maus, S., Gordon, D., and Fairhead, D., 1997. Curie temperature depth estimation using a self-similar magnetization model, Geophys. J. Int., 129, 163– 168, doi:10.1111/j.1365-246X.1997.tb00945.x.

Maus, S., Sazonova, T., Hemant, K., et al., 2007. National Geophysical Data Center candidate for the World Digital Magnetic Anomaly Map. Geochemistry, Geophys. Geosystems 8, n/a–n/a. doi:10.1029/2007GC001643.

Mayhew, M.A., Johnson, B.D., Wasilewski, P., 1985. A review of problems and progress in studies of satellite magnetic anomalies. J. Geophys. Res. 90, 2511–2522.

Miura, S., Kodaira, S., Nakanishi, A., Tsuru, T., Takahashi, N., Hirata Naoshi, Kaneda, Y., 2003. Structural characteristics controlling the seismicity of southern Japan Trench fore-arc region, revealed by ocean bottom seismographic data, Tectonophysics, 363, 79-102, doi: 10.1016/S0040-1951(02)00655-8.

Münch Ph., Cornee J.-J., Lebrun J.-F., Quillevere F., Verati C., Melinte-Dobrinescu M., Demory F., Smith B., Jourdan F., Lardeaux J.-M., De Min L., Leticee J.-L., Randrianasolo A., 2014. Pliocene to Pleistocene vertical movements in the forearc of the Lesser Antilles subduction: insights from chronostratigraphy of shallow-water carbonate platforms

(Guadeloupe archipelago). Journal of the Geological Society, doi.org/10.1144/jgs2013-005.

Mutter, C.Z., Mutter, J.C., 1993. Variations in thickness of layer 3 dominate crustal structure oceanic. Earth Planet. Sci. Lett. 117, 295 –317.

Nagle, F., 1972. Rocks from seamounts and escarpments on the Aves Ridge, in: Trans. 6th Caribbean Geol. Conf. Caracas, pp. 409–413.

Officer, C. B., Ewing, J. L., Hennion, J. F., Harkrider, D. G., Miller, D. E., 1959. Geophysical investigations in the eastern Caribbean: Summary of 1955 and 1956 cruises, Phys. Chem. Earth, 3, 17–109, doi:10.1016/0079-1946(59) 90004-7.

Okubo, Y., Graff, R.G., Hansen, R.O., et al., 1985. Curie point depths of the Island of Kyushu and surrounding areas. Geophysics 51, 481–494.

Okubo, Y., Tsu, H., Ogawa, K., 1989. Estimation of Curie point temperature and geothermal structure of island arcs of Japan. Tectonophysics 159, 279–290. doi:10.1016/0040-1951(89)90134-0

Parsons, B., Sclater, J.G., 1977. An analysis of the variation of ocean floor bathymetry and heat flow with age, J. Geophys. Res., 82, 803-827.

Pecknold, S., Lovejoy, S., and Schertzer, D., 2001. Stratified multifractal magnetization and surface geomagnetic fields-II. Multifractal analysis and simulations, Geophys. J. Int., 145, 127–144, doi:10.1111/j.1365-246X. 2001.00345.x.

Pilkington, M., Todoeschuck, J. P., and Gregotski, M. E., 1994. Using fractal crustal magnetization models in magnetic interpretation, Geophys. Prospect., 42, 677–692, doi:10.1111/j.1365-2478.1994.tb00235.x.

Pollack, H.N., Hurter, S.J., Johnson, J.R., 1993. Heat loss flow from the earth's interior: analysis of the global data set. Rev. Geophys. 31, 267–280.

Quarta, T., Fedi, M., De Santis, A., 2000. Source ambiguity from an estimation of the scaling exponent of potential field power spectra. Geophysical Journal International, 140(2), 311-323.

Rajaram, M., Anand, S.P., Hemant, K., et al., 2009. Curie isotherm map of Indian subcontinent from satellite and aeromagnetic data. Earth Planet. Sci. Lett. 281, 147–158. doi:10.1016/j.epsl.2009.02.013

Ranally, G., and Murphy, D., (1987) Geological stratification of the lithosphere. Tectonophysics 132: 281–295.

Ranero, C. R., Phipps Morgan, J., McIntosh, K., Reichert, C., 2003. Bending-related faulting and mantle serpentinization at the Middle America trench, Nature, 425, 367-373.

Ravat, D., Pignatelli, A., Nicolosi, I., Chiappini, M., 2007. A study of spectral methods of estimating the depth to the bottom of magnetic sources from near-surface magnetic anomaly data. Geophys J Int 169:421-434.

Ravat, D., Salem, A., Abdelaziz, M.S., et al., 2011. Probing magnetic bottom and crustal temperature variations along the Red Sea margin of Egypt. Tectonophysics 510, 337–344. doi:10.1016/j.tecto.2011.08.002.

Ross, H. E., Blakely, R. J., and Zoback, M. D., 2006. Testing the use of aeromagnetic data for the determination of Curie depth in California, Geophysics, 71, L51, doi:10.1190/1.2335572.

Roux, E., 2007. Reconnaissance de la structure sismique de la zone de subduction des Petites Antilles (Guadeloupe et Martinique). Paris VII-Denis Univ, Diderot.

Ruiz, M., Galve, A., Monfret, T., Sapin, M., Charvis, P., Laigle, M., Evain, M., Hirn, A., Flueh, E., Gallart, J., Diaz J., Lebrun, J.-F., and the Lesser Antilles Thales scientific party, 2013. Seismic activity offshore Martinique and Dominica islands (Central Lesser Antilles

subduction zone) from temporary onshore and offshore seismic networks, Tectonophysics, 603, 68-78, doi: 10.1016/j.tecto.2011.08.006

Saad, A.F., Magnetic properties of ultramafic rocks from Red Mountain, California. Geophysics, v. 34, p. 974–987.

Salem, A., Green, C., Ravat, D., et al., 2014. Depth to Curie temperature across the central Red Sea from magnetic data using the de-fractal method. Tectonophysics 624-625, 75–86. doi:10.1016/j.tecto.2014.04.027

Schubert, C.E., Peter, G., 1974. Heat flow northeast of Guadeloupe Island, Lesser Antilles. J. Geophys. Res. 79, 2139–2140.

Schmidt, M.W., Poli, S., 1998. Experimentally based water budgets for dehydrating slabs and consequences for arc magma generation, Earth Planet. Sci. Lett., 163, 361-379.

Sevilla, W. I., Ammon, C. J., Voight, B., De Angelis, S., 2010. Crustal structure beneath the Montserrat region of the Lesser Antilles island arc, Geochem. Geophys. Geosyst., 11, Q06013, doi:10.1029/2010GC003048.

Shuey, R.T., Shellinger, D.K., Tripp, A.C., et al., 1977. Curie depth determination from aeromagnetic spectra. Geophys. J. R. Astron. Soc. 50, 75–101.

Spector, A., Grant, S., 1970. Statistical models for interpreting aeromagnetic data. Geophysics 35, 293–302.

Stacey, F.O., 1977. Physics of the Earth. John Wiley and Sons, New York.

Stüwe, K., 2002. Geodynamics of the Lithosphere. Springer-Verlag, Berlin, 449 pp.

Suyehiro, K., Takahashi, N., Ariie, Y., et al., 1996. Continental Crust, Crustal Underplating, and Low-Q Upper Mantle Beneath an Oceanic Island Arc. Science (80-.). 272, 390–392. doi:10.1126/science.272.5260.390

Symithe, S., Calais, E., de Chabalier, J.B., Robertson, R., Higgins, J., 2015. Current block motions and strain accumulation on active faults in the Caribbean, J. Geophys. Res., 120, 3748-3774.

Takahashi, N., Kodaira, S., Klemperer, S.L., et al., 2007. Crustal structure and evolution of the Mariana intra-oceanic island arc. Geology 35, 203. doi:10.1130/G23212A.1

Tanaka, A., Okubo, Y., Matsubayashi, O., 1999. Curie point depth based on spectrum analysis of the magnetic anomaly data in East and Southeast Asia. Tectonophysics 306, 461–470. doi:10.1016/S0040-1951(99)00072-4

Tomblin, J.F., 1975. The Lesser Antilles and Aves Ridge, in: Nairn, A.E.M., Stehli, F.G. (Eds.), The Ocean Basins and Margins, Vol. 3, The Gulf of Mexico and the Caribbean. New York, N.Y., pp. 467–500.

Tsokas, G., Hansen, R.O., Fyticas, M., 1998. Curie Point Depth of the Island of Crete (Greece). Pure appl. Geophys. 152, 747–757.

Turcotte, D., Schubert, G., 2002. Geodynamics second edition. Cambridge University Press, 2002.

Uchida, Supraslab earthquake clusters above the subduction plate boundary offshore Sanriku, northeastern Japan: Seismogenesis in a graveyard of detached seamounts? J. Geophys. Res., 115, B09308, doi:10.1029/2009JB006797.

Uyeda, S., Kirby, S.H., Okada, T., Hino, R., Hasegawa, A., 1984. Subduction zones: their diversity, mechanism and human impacts. GeoJournal, 8.4, 381-406.

van Keken, P.E., King, S.D., Schmeling, H., Christensen, U.R., Neumeister, D., M.-P. Doin, 1997. A comparison of methods for the modeling of thermochemical convection, J. Geophys. Res., 102, 22477-22495.

van Keken, P.E., Kiefer, B., Peacock, S.M., 2002. High-resolution models of subduction zones: implications for mineral dehydration reactions and the transport of water into the deep mantle, Geochem. Geophys. Geosyst., 3, doi: 10.1029/2001GC000256, 1056.

Wasilewski, P., Mayhew, M.A., 1992. The Moho as a magnetic boundary revisited. Geophys. Res. Lett. 19, 2259–2262.

Wasilewski, P., Thomas, H.H., Mayhew, M.A., 1979. The Moho as a magnetic boundary. Geophys. Res. Lett. 6, 541–544.

Westbrook, G.K. and McCann, W.R., 1986. Subduction of Atlantic lithosphere beneath the Caribbean. In: P.R. Vogt and B.E. Tucholke,Eds., The geology of North America, M, The western North Atlantic region. Geol. Soc. Amer, 341-350.

Westercamp, D., 1979. Divertsité, contrôlestructural et origines du volcanisme récent dans l'arc insulaire des Petites Antilles. Bull. Bur. Rech. Géol. Min. Fr. IV, 211–226.

Whitmarsh, R. B., Keen, C. E., Steinmetz, L., Tomblin, J., Donegan, M., Lilwall, R. C., Loncarevic, B. D., Nichols, B., Shepherd, J., 1983. A lithospheric seismic refraction profile in the western North Atlantic Ocean, Geophys. J. R. Astron. Soc., 75, 23–69.

Wilks, K.R., and Carter, N.L. (1990) Rheology of some continental lower crustal rocks. Tectonophysics, 182, 57–77.

Figure 1

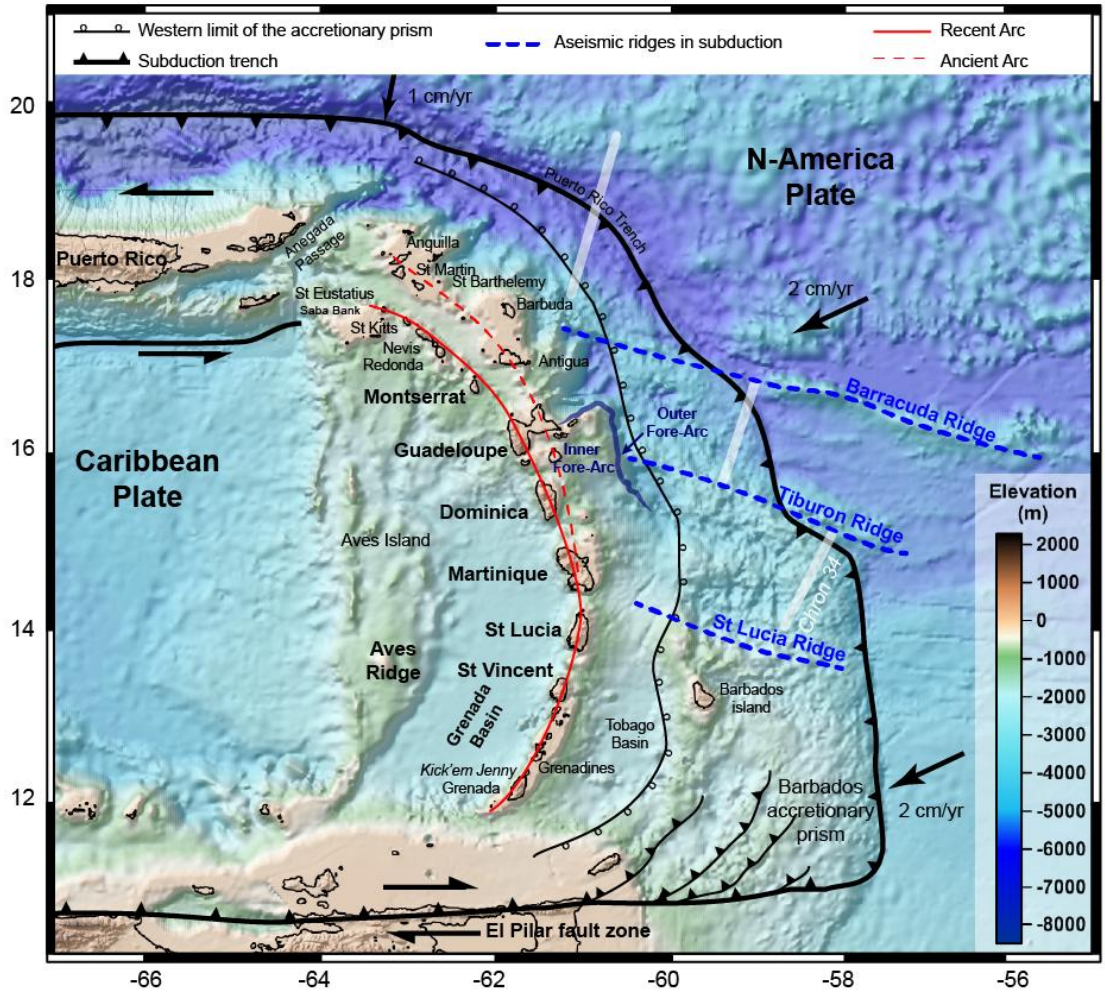

Large scale context of the LAA (after [*Bouysse and Westercamp*, 1988]).

Figure 2

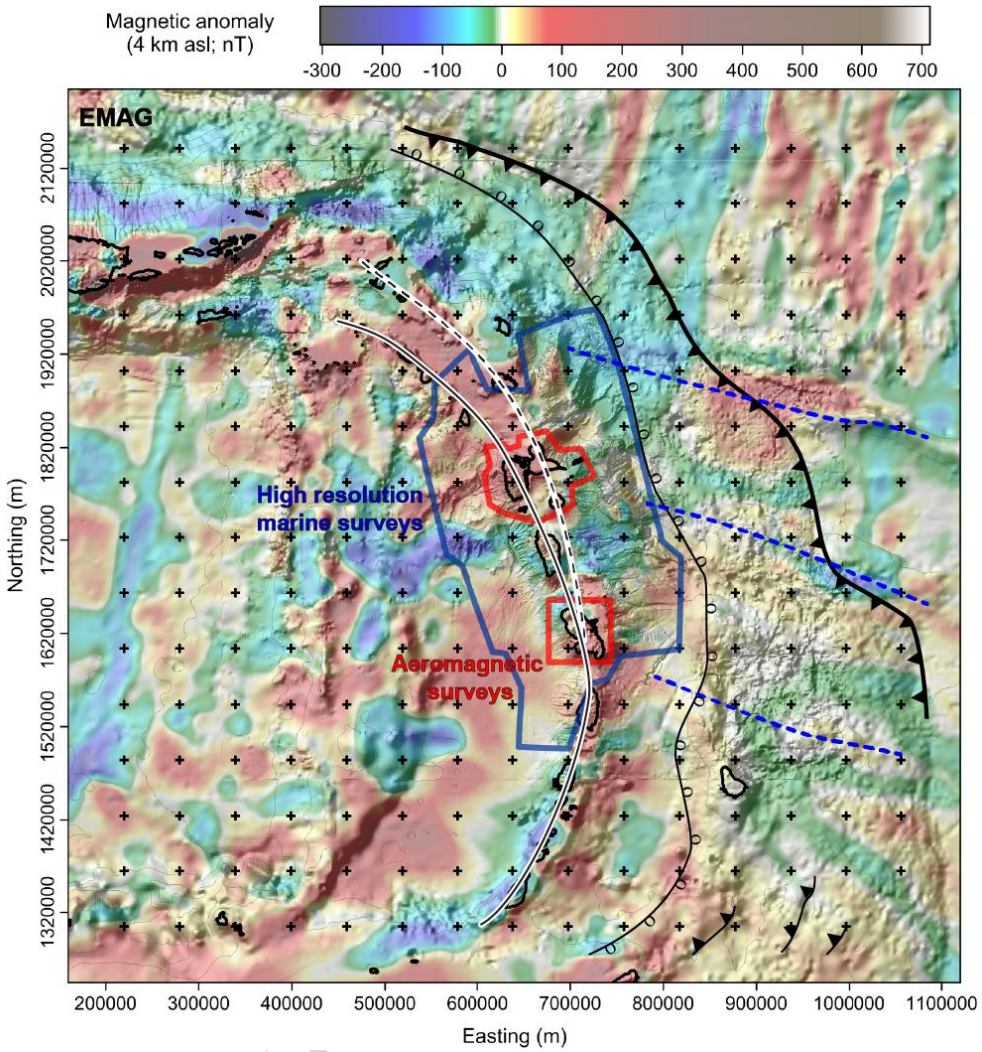

Magnetic anomaly map computed at 4 km a.s.l. (cell size 470 m) from the compilation of the aeromagnetic survey [*LeBorgne and LeMouel*, 1976] marine dataset [*Gailler et al.*, 2013] and EMAG-V2 [*Maus*, 2009]. The location of the various datasets is shown in the right-bottom side. The black solid contours refer to the 0 m isobaths. The black crosses locate the center of each CPD computation window (120 x 120 km; Fig. 3). The underlying shaded large scale bathymetry is extracted from ETOPO model (1 arc-minute global relief model of Earth's surface that integrates land topography and ocean bathymetry) available from the NOAA database at http://www.ngdc.noaa.gov/mgg/global/global.html). Coordinates in kilometers (WGS84, UTM 20N).

Figure 3

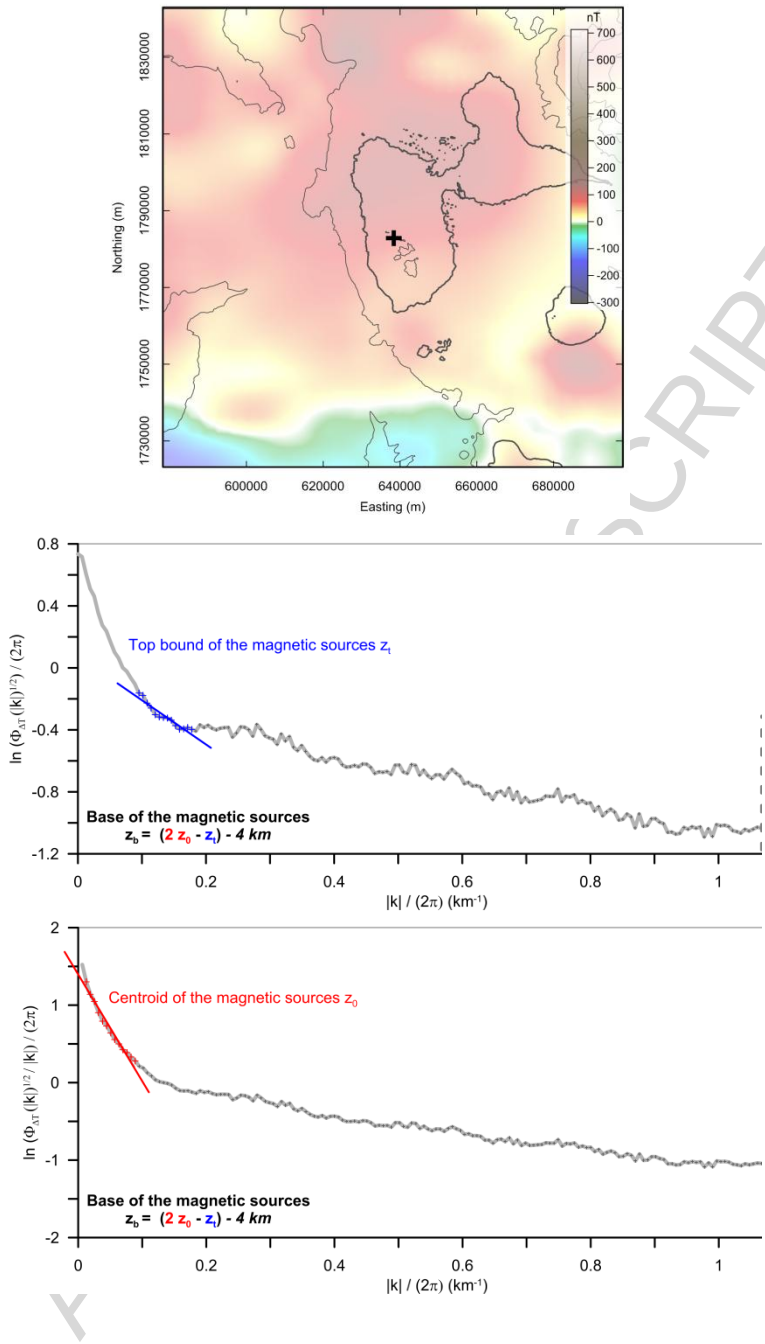

Example of azimuthally averaged power spectra for the estimation of the depth to the magnetic bottom using the two-dimensional upward continued magnetic anomaly data (data covering the 120x120 km subregion centered on 638.125-1782.890 km, located on top). According to Tanaka et al. (1999), z_0 and zt are defined as the centroid and the top bound of the magnetic sources respectively (|k| is the wavenumber and $\phi_{\Delta T}$ (|k|) is the spectrum of the magnetic anomaly). The main slopes and the noise level are underlined on each graph.

Figure 4

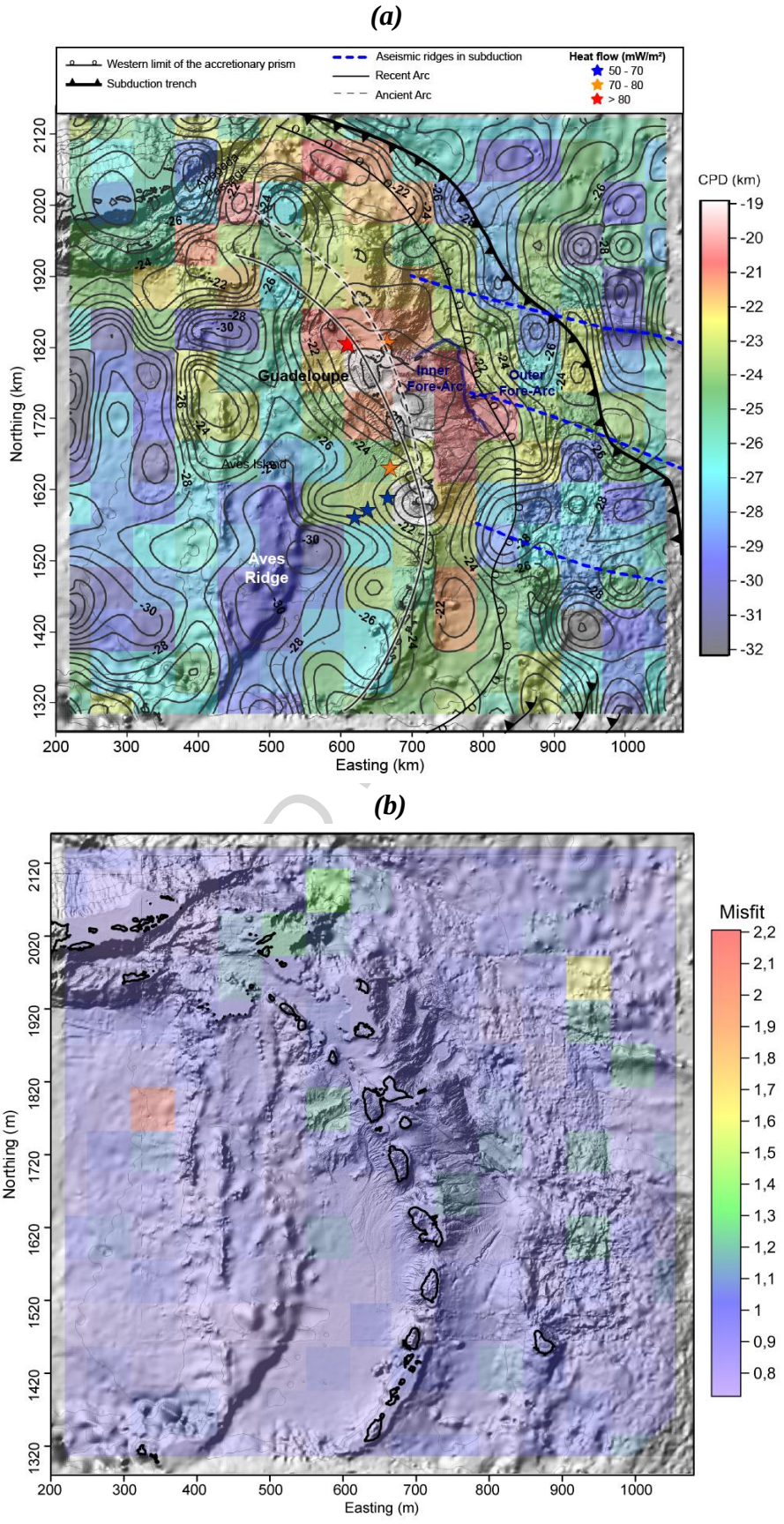

(c)

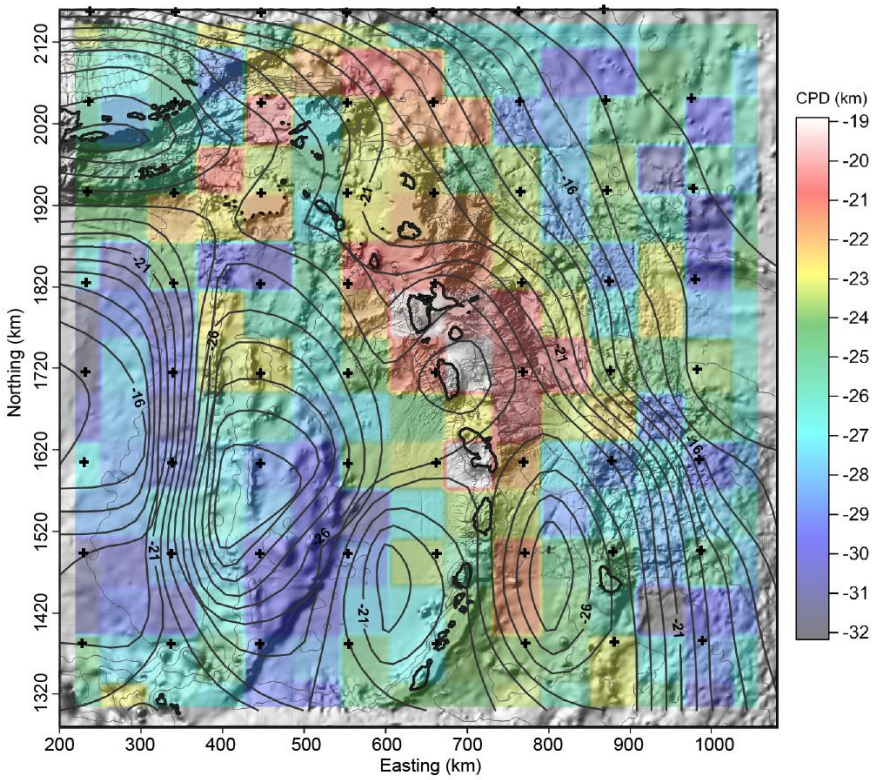

a) Calculated CPD map represented by both color-coded square windows and interpolated contours. The main structural features are located. Heat flow measurements are located by stars [*Manga et al.*, 2012]. **b)** Map of the misfit (eq. 3) between the theoretical curve and the radial power spectra (Fig. 3). For the calculation of the theoretical curve (eq. 2), we used the estimated values of z_t and $\Delta z=z_b-z_t$. For the entire area,the root-mean-square (RMS) of the misfit value is equal to 0.92. **c)** Depth to Moho relative to sea level are extracted from Crust1.0 model [*Laske et al.*, 2013]. Coordinates in kilometers (WGS84, UTM 20N).

Figure 5

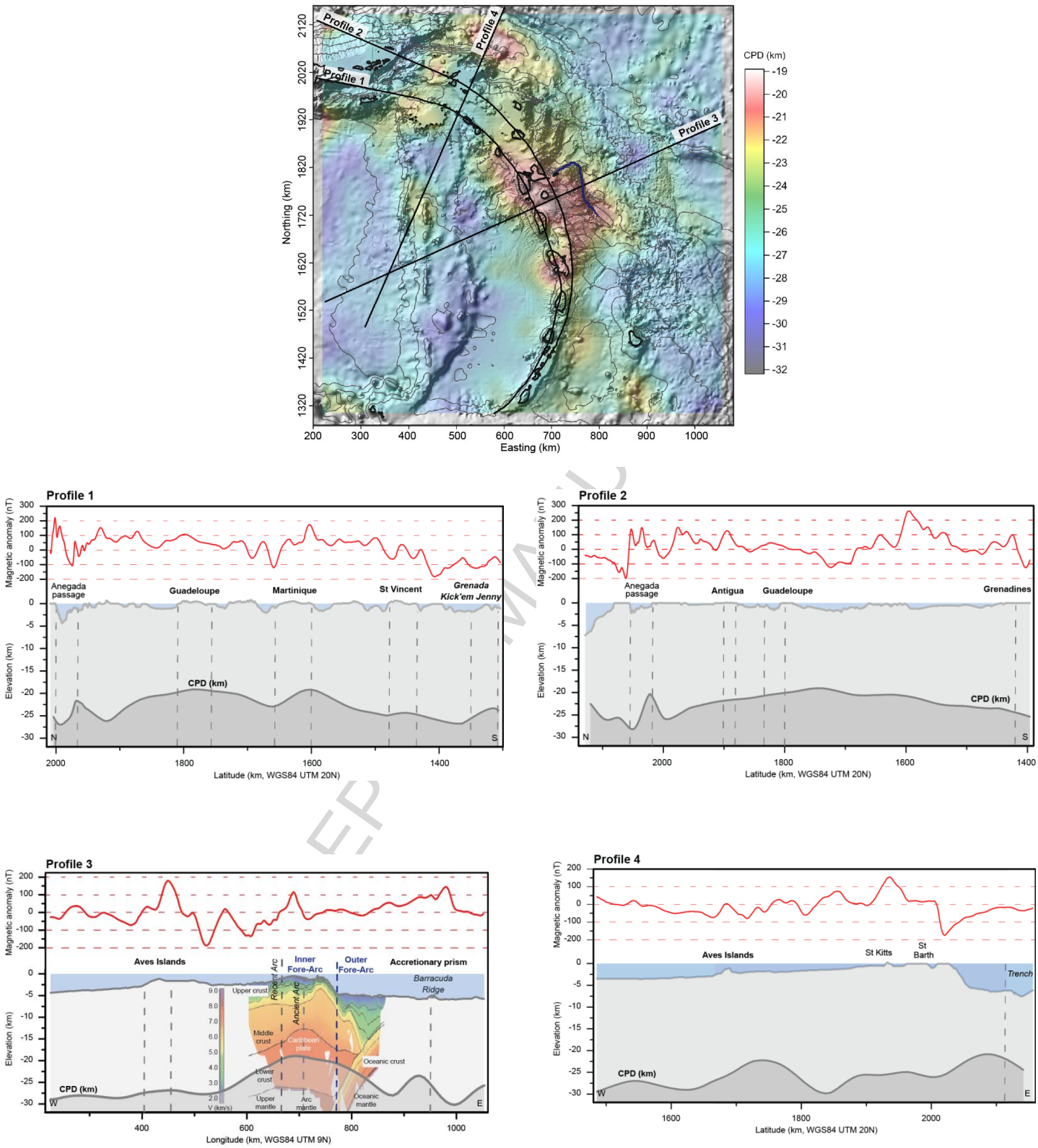

Comparison between CPD estimates and bathymetry along four main profiles of interest located in the CPD map on top.

Figure 6

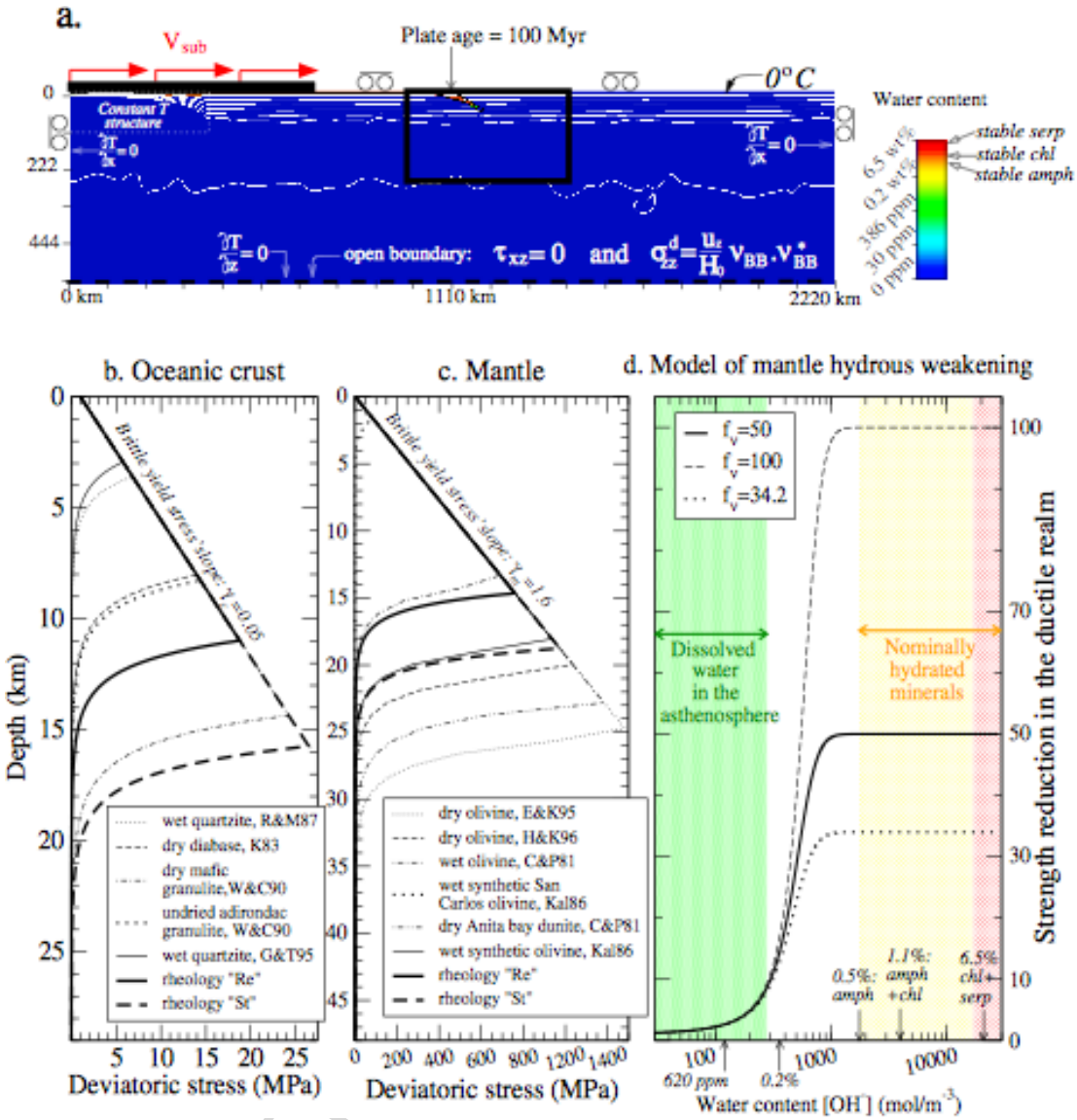

a) Geometry of the simulation box and boundary conditions. The inserted black box represents both the region where the numerical mesh is refined and the close-up displayed in panels b and c. **Panels b and c :** Simulated rheologies (labels «Re» and « St ») versus experimentally determined rheologies for crustal compositions (a) and mantle rocks (b). Stress profiles are computed for a 100 km thick lithosphere geotherm and a uniform reference strain rate equal to 10^{-14} s^{-1}. « R&M87 »: *Ranally and Murphy* [1987]; «K83 »: *Kirby* [1983]; «W&C90» : *Wilks and Carter* [1990]; «G&T95»: *Gleason and Tullis* [1995]; «E&K95»: *Evans and Kohlstedt* [1995]; «H&K96»: *Hirth and Kohlstedt* [1996]; «C&P81»: *Chopra and Paterson* [1981]; «Kal86»: *Karato et al.* [1986]. **Panel d**: Modeled strength reduction for the ductile mantle as a function of water content. The water content scale is displayed in mol/m^3, but corresponding values in weight percent are indicated. amph : stable amphibole; chl : stable chlorite; serp: stable serpentine. Colors refer to the color scale of water content used in panel a.

Figure 7

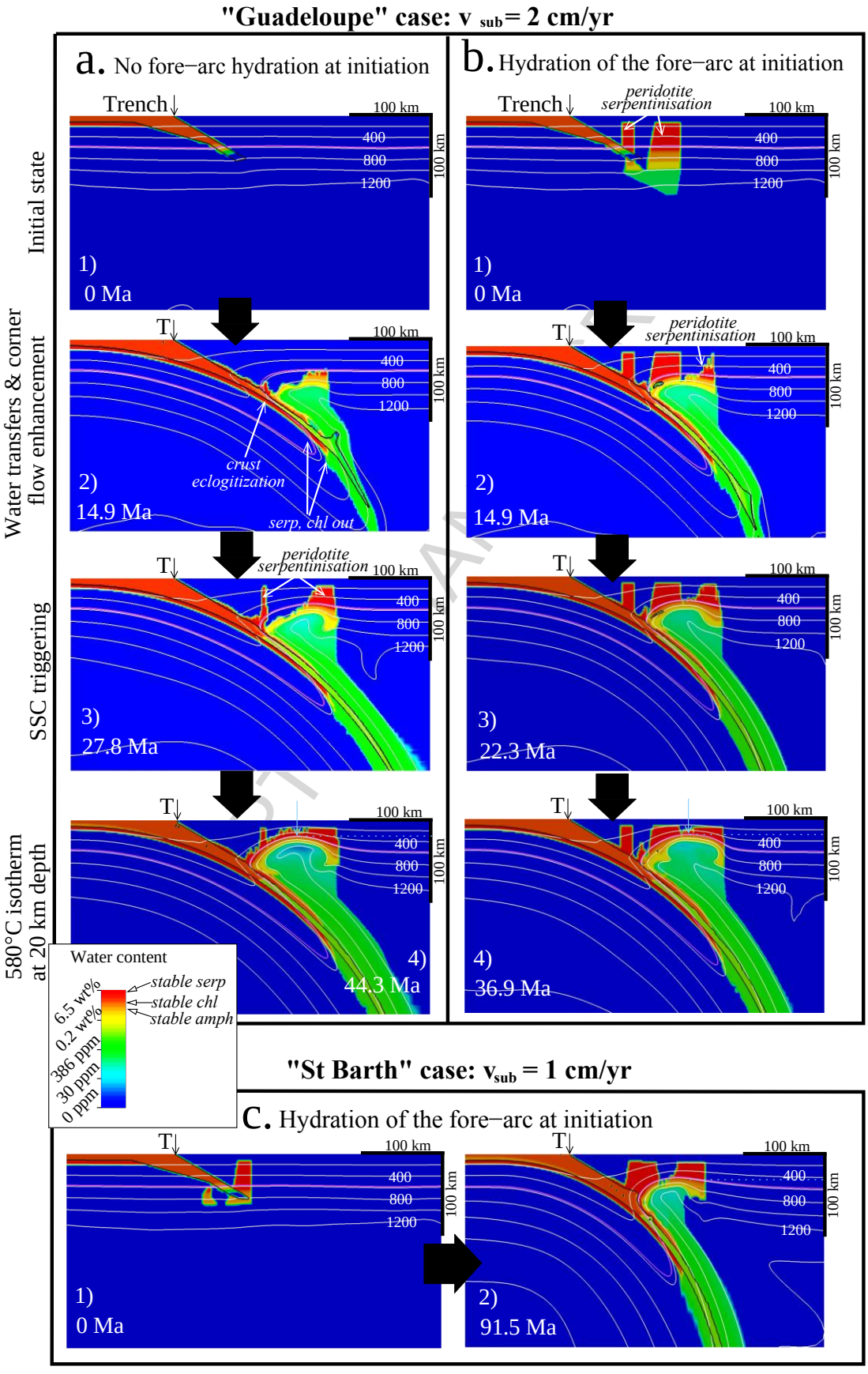

Panels a1-4: Simulation G4 with a 2 cm/yr convergence rate when no hydration is imposed in the upper plate at convergence start (rheology Re and f_v=50). **Panels b1-4**: Simulation G5 with a 2 cm/yr convergence rate and an initial water-saturation in the fore-arc domain at convergence start (rheology Re and f_v=50). **Panels c1-2**: Simulation SB5 with a 1 cm/yr convergence rate and an initial fore-arc hydration at convergence start (rheology Re and f_v=50). Isotherms (white lines) are depicted every 200°C. The pink line is the 580°C isotherm. The black outline delimits the subducting 'crustal' layer. Blue arrows indicate the location of the shallowest depth of the 580°C isotherm. «T » : trench location.

Figure 8

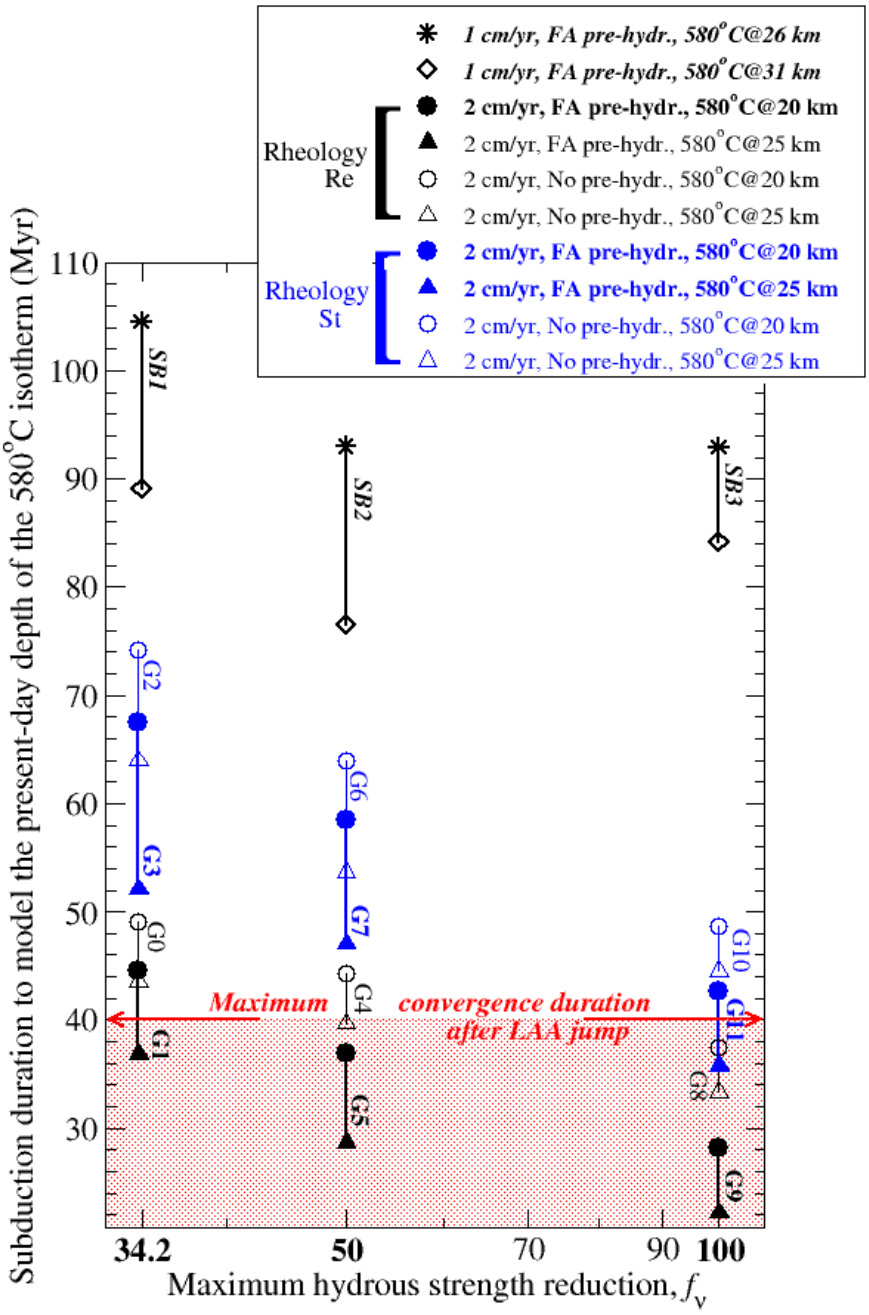

Characteristic times of fore-arc lithosphere heating, measured as the duration of convergence necessary to model the 580°C isotherm shallowing within the overriding lithosphere up to either 20 km depth (profile 3 modeling, 2 cm/yr) or 26 km (profil 4 modeling, 1 cm/yr), as a function of the maximum amount of water-related weakening, $f_{\square}$. 'FA pre-hydr': Fore-arc pre-hydration imposed at simulation initiation. 'No pre-hydr': No pre-hydration of the fore-arc mantle imposed at convergence start.

Figure 9

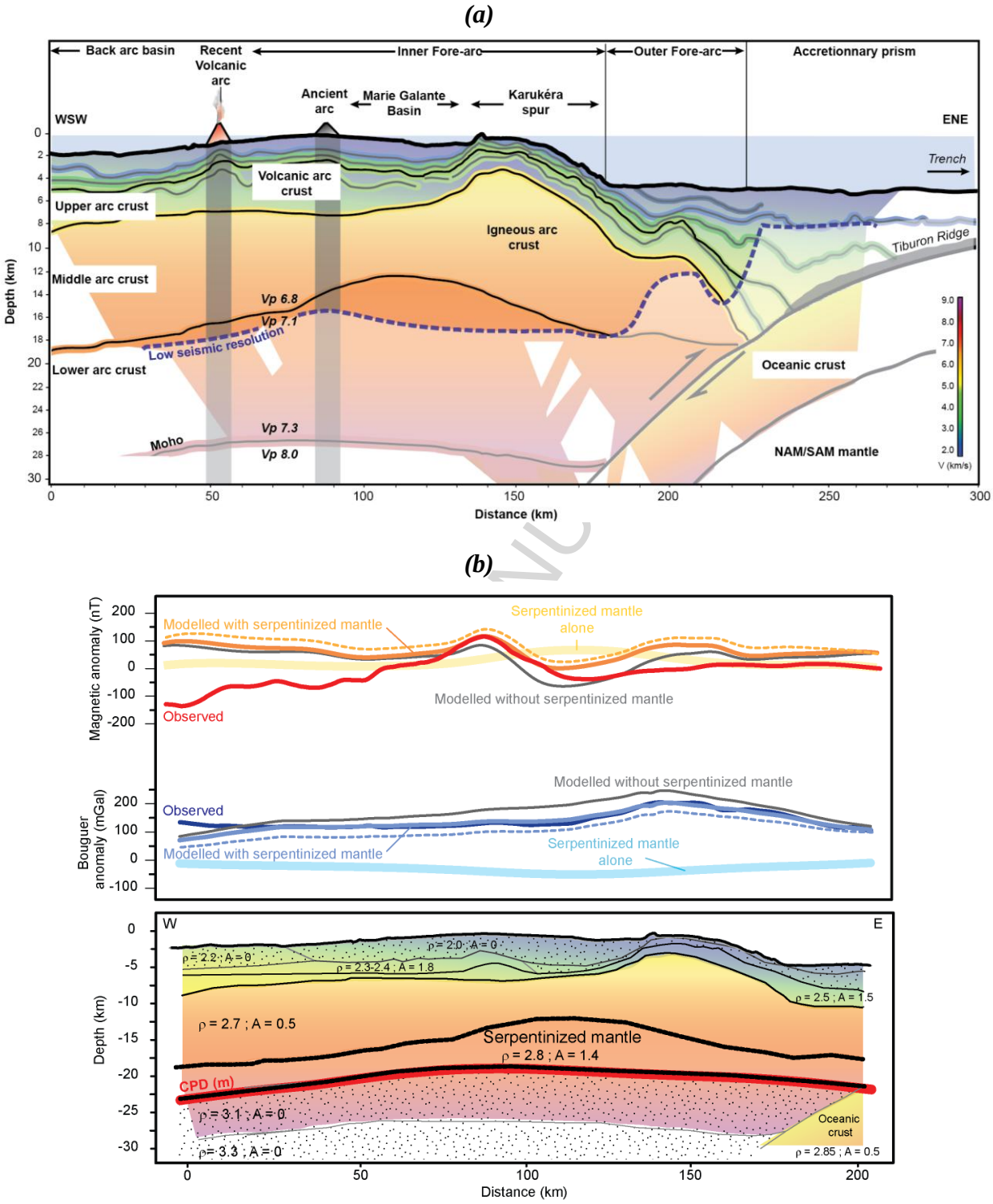

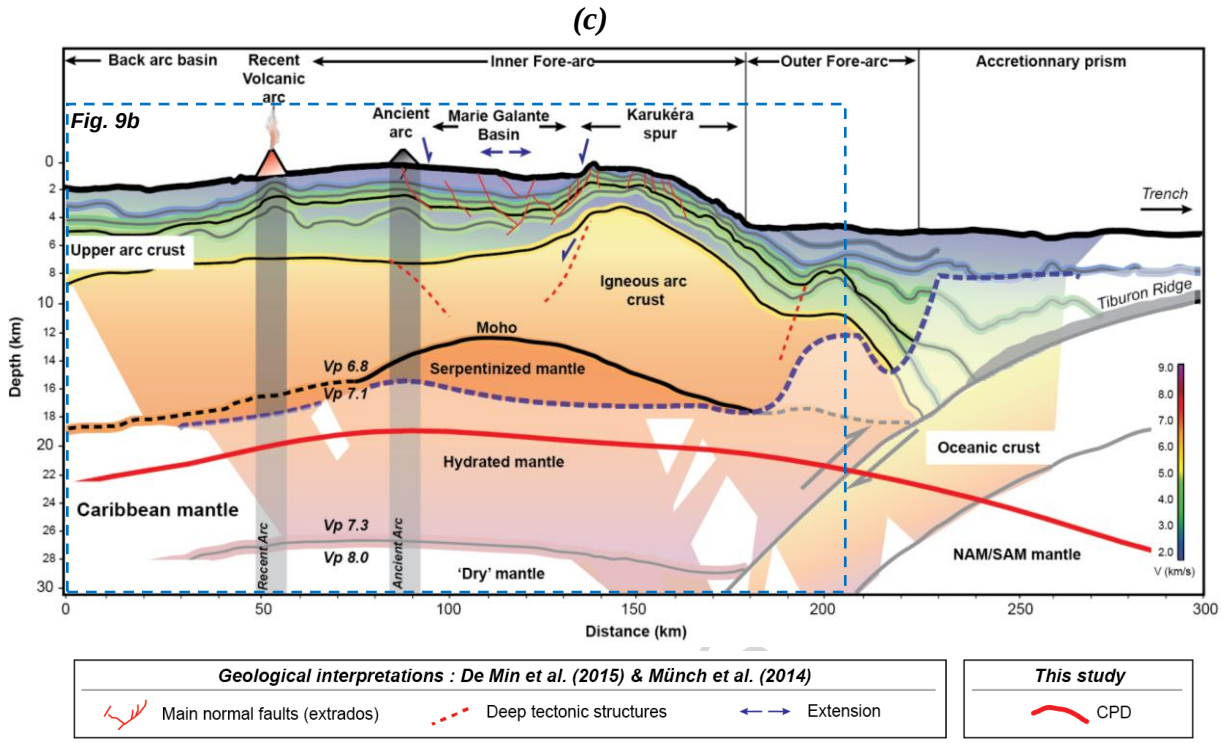

a) 2D velocity model across the Lesser Antilles island arc [*Kopp et al.*, 2011]. The dashed blue line underlines the upper bound of the low resolution of the seismic rays (bleached downward). **b)** Simultaneous gravity and magnetic model along the 2D velocity model. Upper panel: thick lines labeled 'serpentinized mantle alone' refer to gravity and magnetic response of a serpentinized crust alone. Dashed lines refer to models considering a CPD 5km deeper, corresponding to the overall uncertainty on our estimation. Lower panel: dotted areas locate the paramagnetic layers. See Table 3 for physical properties used in model (ρ: density in 10^3 $kg.m^{-3}$; A: magnetization in $A.m^{-1}$). The magnetic profile is extracted from the map presented in this study. The gravity profile is extracted from the gravity map computed by *Gailler et al.* [2013]; **c)** New interpretation along the seismic profile from *Kopp et al.* [2011] derived from this study and the recent geological considerations from *De Min et al.* [2015] and *Münch et al.* [2014].

Table 1.

Structures near	Reference	Moho depth	CPD (this study)
Guadeloupe	*Boynton et al.* [1979]	30 km	19-22 km
St Vincent	*Boynton et al.* [1979]	35 km	22-25 km
Barbuda	*Whitmarsch et al.* [1983]	28 km	22-23 km
Grenada	*Christeson et al.* [2008]	25 km	26-28 km
Martinique	*Sevilla et al.* [2010]	32 km	19-22 km

CPD and Moho depth comparison in the study area.

Table 2

Unit		Averaged density (10^3 kg.m^{-3})		Averaged magnetization (A.m^{-1})	
As defined by Kopp et al. [2011]	**As interpreted in this study**	**No serpentinized mantle**	**Serpentinized mantle**	**No serpentinized mantle**	**Serpentinized mantle**
Voclanic Arc crust	***Sediments***	2.0-2.2		0	
	Voclanic Arc crust	2.3-2.4		1.8	
Upper arc crust	***Upper arc crust***	2.5		1.5	
Middle arc crust	***Igneous arc crust***	2.7		0.5	
Lower arc crust	***Serprentinized mantle***	3.1	2.8	0	1.4
	Hydrated mantle		3.1		0
Oceanic crust	***Oceanic crust***	2.85		0.5	
Upper mantle	***Dry mantle***	3.3		0	

Physical properties used in gravity and magnetic models (Fig. 9b).

RESEARCH HIGHLIGHTS

> Curie Point Depth estimation at the scale of the Lesser Antilles Arc

> Main doming below Guadeloupe archipelago, suggesting a very hot state of the fore-arc/arc domains

> 2D thermo-mechanical simulations of the thermal structure of the arc lithosphere

> Serpentinized, therefore highly magnetized lithospheric fore-arc wedge

> Moho at shallower depth than previously expected